Ocean Engineering 343 (2026) 123168

Contents lists available at ScienceDirect

Ocean Engineering

journal homepage: www.elsevier.com/locate/oceaneng

Research paper

Boundary element methods in action: A performance assessment for ocean engineering applications

I. Zabala [a], T.E. Kelly [b], J.C.C. Henriques [c], Y. Peña-Sanchez [d], M. Penalba [d,e], J.M. Blanco [f,*]

[a] SENER Ingeniería y Sistemas, S.A. Zugatzarte Etorb. 56, Getxo, Spain
[b] Dundalk Institute of Technology, Marshes Upper, Dundalk, Co. Louth, A91 K584, Ireland
[c] LAETA, IDMEC, Instituto Superior Técnico, Universidade de Lisboa, Av. Rovisco Pais, Lisboa, 1049-001, Portugal
[d] Mondragon University, Loramendi Kalea 4, Arrasate, 20500, Spain
[e] Ikerbasque Basque Foundation for Science, Euskadi Plaza 5, Bilbao, 48009, Spain
[f] University of the Basque Country, Plaza Ingeniero Torres Quevedo, 1, Edif. I, Bilbao, 48993, Spain

ARTICLE INFO

Keywords:
Marine renewable energy
Seakeeping problem
Boundary element method

ABSTRACT

Boundary Element Method (BEM) solvers play a key role in industrial-level marine device research. Despite relying on simplified hydrodynamic models, their computational efficiency and well-established validation has resulted in the widespread adoption of these software tools. These solvers have been created by different authors who, in some instances, have used different approaches to achieve the same objectives, which can lead to unexpected discrepancies in results obtained from different solvers. Some of these differences may not be apparent to the general user. To support an informed selection of software, this work presents a comprehensive review of several widely-used solvers. Their performance was assessed across diverse marine devices using specific metrics, enabling a thorough comparison of key parameters. It has been observed that the most accurate results are obtained by WAMIT and ORCAWAVE, closely followed by HAMS and CAPYTAINE. On the other hand, the most computationally efficient solvers are WAMIT, NEMOH and AQWA, followed by HAMS. As this study is open to the scientific community, all comparative models and pre- and post-processing routines have been shared openly to facilitate the reproducibility of the results, and future iterations of the study, as new versions of the compared software are released.

1. Introduction

The oceans are a complex environment where important economic activities, such as the transport of goods and the extraction of natural resources, take place. These activities are being expanded with the development of floating wind and wave power plants. In order to design devices that perform these activities, it is necessary to predict the loads that they will be subjected to under different operating conditions and in the geographical locations where they will perform their tasks. The numerical models that, due to the precision and industrial quality of their results, best meet these requirements are simulations using Computer Fluid Dynamics (CFD), in particular models based on the Navier-Stokes equations (Penalba et al., 2017a). However, the computational expense of such models drive developers to use other, less accurate models. Such models can, with suitable adjustments, sufficiently reproduce the required wave and loading situations. For this task, potential flow models, based on the Boundary Element Method (BEM), have proven their quality and efficiency.

Solving the seakeeping problem, a key issue in hydrodynamics, is the overall objective of a BEM solver. This problem is concerned with bodies that are fixed, or moving at a forward speed, while being subjected to sinusoidal waves. Such bodies may be partially submerged (floating) or entirely submerged in fluid of infinite or limited depth. The three-dimensional radiation-diffraction problem results from the problem's mathematical formulation (Newman, 1977; Liang and Chen, 2025).

There are numerous software packages that perform the previously outlined functions, so the researcher or engineer must choose the most appropriate tool to support the device being designed. To help in this decision, several studies have been published on this topic. In order not to implicitly give more importance to some software over others, and since in most cases, the original meaning of the acronyms has lost its

* Corresponding author.
E-mail addresses: inaki.zabala@energy.sener (I. Zabala), thomas.kelly@dkit.ie (T.E. Kelly), joaochenriques@tecnico.ulisboa.pt (J.C.C. Henriques), ypena@mondragon.edu (Y. Peña-Sanchez), mpenalba@mondragon.edu (M. Penalba), jesusmaria.blanco@ehu.eus (J.M. Blanco).

https://doi.org/10.1016/j.oceaneng.2025.123168
Received 1 July 2025; Received in revised form 22 September 2025; Accepted 11 October 2025
Available online 27 October 2025

Romans

A	added mass matrix [kg, kg m^2]
B	radiation damping matrix [kg/s^2, kg m^2/s]
C	stiffness matrix [kg/s, kg m^2/s^2]
D	number of devices
e	error ratio
j	imaginary unit
K	impulse response function matrix [kg/s^2, kg m^2/s]
M	inertia matrix [kg, kg m^2]
n	number of frequencies
N	number of degrees of freedom
P	number of panels
Re	Reynolds number
t	time [s]
T	period [s]
y	generic hydrodynamic parameter

Greek symbols

ζ	damping ratio
θ	wave heading [deg]
ρ	water density [kg/m^3]
ω	angular frequency [rad/s]

Subscripts

0	zero frequency
∞	infinite frequency
crit	critical
i	degree of freedom
k	index of a device
ref	reference hydrodynamic parameter

Acronyms

BEM	Boundary Elements Method
BVP	Boundary Value Problem
CAD	Computer Aided Design
CFD	Computational Fluid Dynamics
CLI	Command Line Interface
DLL	Dynamic-Link Library
DNV	Det Norske Veritas
ECN	École Centrale de Nantes
EWTEC	European Wave and Tidal Energy Conference
GMRES	Generalized Minimal Residual Method
GPL	General Public License
GUI	Graphical User Interface
IEA	International Energy Agency
IRF	Impulse Response Function
IST	Instituto Superior Técnico
LHEEA	Laboratoire de recherche en Hydrodynamique, Énergétique et Environnement Atmosphérique
MARIN	Maritime Research Institute of the Netherlands
MASK	Manoeuvring and Seakeeping Basin
MEC	Marine Energy Converters
MIT	Massachusetts Institute of Technology
MKL	Math Kernel Library
NREL	National Renewable Energy Laboratory
NRMSE	Normalized Root Mean Square Error
NURBS	Non-Uniform Rational B-Splines
ORE	Offshore Renewable Energy
OSWC	Oscillating Surge Wave Converter
OWC	Oscillating Water Column
PDE	Partial Differential Equations
PTO	Power Take-Off
QTF	Quadratic Transfer Functions
RAE	Relative Absolute Error
RAM	Random-Access Memory
RAO	Response Amplitude Operator
RMS	Root Mean Square
RMSE	Root Mean Square Error
ROPAX	Roll-On/roll-off Passenger
UCD	University College Dublin
WEC	Wave Energy Converter
XCORR	Cross Correlation

significance, the names of all the software used are included in upper case.

Naciri and Sergent (2009) includes a benchmark study for a standard Liquefied Natural Gas Carrier (LNGC), where seven commercial diffraction/radiation software were used for the comparison (AQWA, Delfrac (Jonge et al., 2008), Diffrac (Buchner et al., 2001), Diodore, Hydrostar (Chen, 1993), Wadam and WAMIT). First and second order calculations, including far field mean drift and near field wave drift Quadratic Transfer Functions (QTF), were performed. In that work, the results compared included some of the terms of the hydrostatic stiffness matrix, the free decay periods and damping ratio for heave, roll and pitch, a visual comparison of first order excitation force magnitude and phase, the mean wave drift load in surge, sway and yaw, and the effect of slowly varying the wave drift load QTF. The results for first order parameters were similar despite differences in meshing between solvers. Mean wave drift loads with the far-field method were quite consistently predicted by all the solvers, except at isolated frequencies, but the results calculated with near field method showed significant differences between solvers.

The study described in Silver et al. (2008) includes an evaluation of various multibody ship motion prediction codes, those being Mvs-Csc, Mvtds, AQWA, ShipMo3D (Mctaggart, 2011), AEGIR (Kring et al., 1999), and LAMP-Multi (Large Amplitude Motions Program) (Weems, 2007). Data from a test conducted at the Maritime Research Institute of the Netherlands (MARIN) were correlated with the results of the individual codes. The cases studied focused on the dynamic analysis of two ships positioned parallel to each other. The parameters used to compare the results were the amplitude and phase of the Response Amplitude Operator (RAO) and the added mass. The comparison was done by visual similarity between the graphs of each parameter against wave frequency. In addition, a percentage difference between the model test results were also computed by taking the difference between the predicted RAO amplitude and phase at each frequency and the model test results. The resulting value for the amplitudes were then normalized by dividing the resulting difference by the largest value of amplitude over all headings and frequencies from the model test. The phase difference was normalized by dividing the result by 360. The final results are then multiplied by 100 to yield the percentage difference. Also an average of the absolute values of the percentage differences across the frequencies was obtained. The results of this evaluation showed a variability in the results of 10–20 % in general, a value which increasing greatly in certain cases. In general, it was also observed that codes with a more sophisticated methodology for motion prediction yielded better prediction results by a small margin. The computational effort was not compared in that work.

The previous report (Silver et al., 2008) was extended to include WAMIT in Silver and Hughes (2010), comparing those results with MOSES, AQWA (zero-speed Green's function), LAMP and AEGIR

(Rankine panel methods). A qualitative comparison table was created which included different simulation capabilities for each solver. Further, a model test of two ships in close proximity was performed in the US Navy's Manoeuvring and Seakeeping Basin (MASK), with one of them free to pitch, heave and roll. Five regular and seven irregular wave conditions were selected for the basis of the evaluation. The quantitative comparison method was similar to that used in Silver et al. (2008). The deviation in heave motions in time domain from each of the simulations was shown to be lower than 25 %.

Another study which considered ship modelling was presented in Gourlay et al. (2015), which compared the results obtained for the analysis of cargo ships in shallow water, using the BEM solvers AQWA, GL RANKINE (Söding, 2009), MOSES, OCTOPUS, PDSTRIP (Bertram et al., 2006) and WAMIT, with experiments realised at the Flanders Hydraulics Research. Comparisons in this work included zero and forward-speed cases, the parameter for comparison is the RAO, and the metrics was the average over all frequencies. To assure consistency in the representation, the same model of each of the models were used in each solver, although different ways to generate the mesh were used for different solvers. Due to this, the design, and the number of panels for each mesh of the same ship, is different. No viscous damping was applied to RAO calculation. The benchmarking showed reasonable agreement of numerical predictions with model test results for heave and pitch over the entire range of wave frequencies studied, with a range of errors up to approximately 20 %.

The work described in Gourlay et al. (2015) was further extended in Parisella and Gourlay (2016) to consider NEMOH solver, comparing the results obtained from NEMOH with those from WAMIT. In addition to using the RAO as the comparison parameter, the added mass, radiation damping and excitation forces were also used. Although no metrics are provided, the results show good agreement using a visual comparison.

A number of comparative studies focussing on BEM results for wave energy devices have also been carried out, including (Penalba et al., 2017b) which modelled some real Wave Energy Converter (WEC) devices using simplified geometric representations. In that work, a submerged axisymmetric point absorber (SAPA, similar to CETO), a two-body point absorber (2BPA, similar to OPT PowerBuoy), an Oscillating Surge Wave Converter (OSWC, similar to Aquamarine Oyster), and a floating Oscillating Water Column (OWC, similar to the IST Sparbuoy) were considered. The quantitative parameters used for that comparison were the added mass, radiation damping, exciting force and Impulse Response Function (IRF), the solvers used in the comparison were NEMOH and WAMIT. The parameters used for the comparison are the cross-correlation and Root Mean Square (RMS), and the metrics are the cross correlation correlation, the maximum correlation, and the RMS ratio. A thorough comparative results table was generated. In general, NEMOH's results were found to be similar to those of WAMIT, except in problems containing the interaction between two bodies, or an oscillating column of water. In terms of computational speed, NEMOH was shown to be significantly slower specially for the case with the higher number of panels. All files used in the generation of the results of this study were made publicly available.

A comparative study between AQWA, ORCAWAVE and NEMOH, was carried out in the thesis (Mon, 2021), with a focus on ship design. A mesh convergence analysis was performed in AQWA-FER, taking as a target the results of the finest mesh, and using as a comparison parameter the relative error in the movements of the device with an irregular wave for the six degrees of freedom obtained in a frequency domain analysis. The chosen mesh has a difference of less than 1 % compared to the finest mesh. This mesh was imported into ORCAWAVE, and NEMOH. Neither the meshes used, nor the numerical results of the study, were included. It was, however, stated that the results for the hydrodynamic coefficients and RAO from each of the three solvers were similar.

In Ref. Sheng et al. (2022), a comparative study between WAMIT, NEMOH and HAMS was performed. In that study, WAMIT results were those considered the most reliable and hence formed the basis for the comparison. That research examined three simple floating structures, including a vertical cylinder with circular cross-section, the same cylinder with a thin heave plate in its lower end, and a vertical cylinder with an octagonal cross-section ending in an inverted conical shape at the top. The parameters compared were the added mass, radiation damping, exciting forces and displacement RAO. Due to the simplicity of the geometries, the degrees of freedom analysed were surge, heave and pitch. The criterion for comparison of the results is visual. There is no indication that any mesh convergence analysis was carried out. The results for the first cylinder were very similar between the three solvers. The results between HAMS and WAMIT with and without dipoles were very similar, but NEMOH obtained different results. However, for the third geometry, the results for all the solvers were very similar. In order to analyse the robustness of the solvers for cases with damaged meshes, two anomalies are considered in the second geometry: a truncated mesh and a vertically overlapped mesh. While the first anomaly did not cause problems, the second caused NEMOH's results to be very different from those of other solvers. In the speed comparison, HAMS was slightly faster than WAMIT, but NEMOH was about four times slower than WAMIT. The meshes used in this study have been made publicly available.

Finally, Raghavan et al. (2022) conducted a comparative study on BEM solvers WAMIT, NEMOH and HAMS, for a cylindrical point absorber and an oscillating surge device, both WECs. The effect of the irregular frequency elimination procedure included with HAMS and WAMIT was evaluated. The added mass, radiation damping, exciting forces, and RAO, were used for visual comparison. As in earlier studies, that study considered WAMIT results the most reliable, and hence the results from WAMIT form the basis for the comparison. The numerical results, except for the irregular frequencies, were quite similar between the three solvers. The computational speed of HAMS, due to its efficiency and parallelisation capacity, was similar to that of WAMIT.

The main contributions of this work are as follows:

- **Large-scale benchmark**: An in-depth analysis of many first order radiation-diffraction zero-velocity Green's function software tools, which are used to model a variety of floating devices, totalling close to 1000 cases.
- **Metrics-based conclusions**: The results obtained are analysed and compared using multiple parameters and metrics, to highlight the differences and advantages of each software and to enable a user to make an informed choice as to the most suitable solver for an application. The results show significant variations in the quality of the results and in the use of computational resources among the solvers reviewed.
- **Detailed geometries**: The geometries included for analysis have been generated so as to represent as accurately as possible the real objects modelled, except for the necessary elimination of small appurtenances that make the calculation difficult, and whose hydrodynamic contribution is insignificant.
- **Single source of meshes**: In order to prevent differences arising in results between solvers that are due to differences in the meshes used to represent geometries in each case, a single source of meshes has been used for all solvers.
- **Higher order, high discretization benchmark**: All geometries modelled have also been modelled in WAMIT using the higher order method with very high discretisation meshes defined by B-spline curved surfaces. The use of higher order panels make such results reliable at a high level, and hence these results serve as a reference for the current study.
- **Reproducibility of all the study**: To allow other researchers to reproduce the results of this study, to add new devices and software tools, and to facilitate updating in the face of continuous software changes and improvements, all the background information for this study has been published and is available to the scientific community. This includes the Computer Aided Design (CAD) models, all

the starting, intermediate and final models for each of the solvers and devices, and the source code and binaries of the pre- and post-processing routines. Such pre- and post-processing routines are necessary, given the large amount of data involved.

It should be noted that, in order to guarantee the integrity of the calculations and conclusions made in this study, the developers of the software tools used have not been given the opportunity to provide any feedback on this study, limiting the contact between them and the authors of this paper to normal technical support in the use of the software through the channels opened by the developers.

The current study employs both commercial and open source software. In the latter, the binaries are distributed for free use, multiple papers can be found indicating their authors and describing their methods, and the source code is accessible and reusable within the fairly permissive limits of each licence. This facilitates scientific progress by making problem-solving strategies explicitly visible. The set of solvers included in this study has been limited by the availability of commercial licences on the part of the authors. As a result, software such as HYDROSTAR could not be included. New phases of this study may involve broader collaborations that would allow additional software to be incorporated.

The work is structured as follows: Section 2 includes a description of each of the solvers included in this study and Section 3 describes the devices used as example cases. Section 4 reviews the conditions under which this study was conducted. Section 5 analyses the reasons why a BEM solver may not perform well in its calculations, reviewing, at a general level, the factors that can be measured to deduce the quality of the results. Section 6 analyses in detail each of the parameters and metrics studied, tabulates the results, and gives possible explanations for the deviations found. Finally, Section 7 reviews other parameters that are not directly related to the quality of the results, but have an impact on the practical functionality of the solvers.

2. Description of the solvers

A general description of each of the solvers included in this study is given below. In addition, Table 1 presents the availability, or otherwise, of specific features in each solver, these features being:

- A_0, A_∞: Calculation of the added mass at frequency at zero and infinite frequency.
- Panel-level info: Panel level output of potentials and/or complex pressures, from which the hydrodynamic coefficients are obtained.
- RAO: Response amplitude operator calculation.
- Irreg. frequen.: Irregular frequencies removal.
- Multi-body analysis: Capability of performing calculations of a multi-body system where there are interactions between the bodies.
- QTF: Quadratic transfer function calculation method. Number 7 refers to control surface/middle field, 8 refers to momentum conservation/far field and 9 refers to pressure integration/near field.
- Higher order: Possibility to perform calculations with meshes based on curved panels.
- Licence type: Commercial (Comm.) or some kind of open licence.
- Automation: Ability to launch a set of calculations from another program or includes a command-line interface (CLI).
- GUI: Graphical User Interface

2.1. AQWA

AQWA (Atkins Quantitative Wave Analysis) is an integrated suite based on hydrodynamics analysis by 3D diffraction/radiation methods. The first version was developed in Fortran by WS Atkins in 1971. Ownership of the software was acquired by Century Dynamics Inc. in 2001. This company was, in turn, acquired by Ansys Inc. in 2005 and now AQWA is integrated into the Ansys Workbench system.

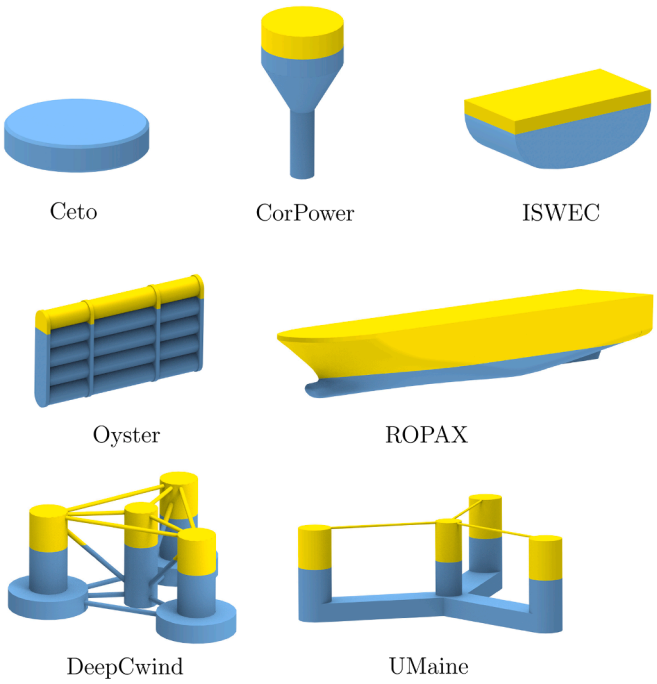

Fig. 1. Representations of the different devices and vessel as they were analysed in this study. The change in the colour indicates the waterline.

Although AQWA includes a graphical user interface, this program maintains access to the classic command line environment, the latter including a finer control of the calculation parameters. AQWA includes an irregular frequency removal algorithm. The software can obtain QTFs using the pressure integration and momentum conservation methods.

2.2. WAMIT

WAMIT (Wave Analysis Massachusetts Institute of Technology) was one of the first panel methods software, developed in Fortran by the researchers S. R. Breit, J. N. Newman, P. D. Sclavounos and C.H. Lee of the Department of Ocean Engineering at the MIT. Its first version was released in 1987. In 1999, WAMIT Inc. was founded by C.H. Lee and J. N. Newman. It uses a boundary-integral formulation based on a variant of the Green's theorem (Newman, 1985) using a combined source and dipole distribution. This capability facilitates the modelling of thin structures, a process that necessitates the resolution of hypersingular integral equations (Martin and Rizzo, 1861). WAMIT has the ability to represent the geometry of the structure not only through flat quadrilateral panels with a uniform source distribution on each panel, but also through higher order curved panels defined as Non-Uniform Rational B-Splines (NURBS) in which the potential is represented by continuous B-splines. To eliminate irregular frequencies, WAMIT has the ability to automatically generates a waterplane mesh (Raghavan et al., 2022), as well as using a user-defined mesh for the waterplane.

2.3. NEMOH and CAPYTAINE

NEMOH is an open source panel method for the computation of first-order hydrodynamic coefficients. It has been in development by the École Centrale Nantes (ECN) for 30 years (Delhommeau, 1989) and is primarily written in Fortran. The first public version (v2.0) was released in January 2014 (Babarit and Delhommeau, 2015) by A. Babarit and G. Delhommeau. Initially it was released under the General Public License (GPL), but soon it adopted the Apache 2.0 license. Unlike other BEM software, NEMOH decouples the resolution of the linear free surface Boundary Value Problem (BVP) from the definition of the boundary

Table 1
Features table. The dash indicates that a feature is not supported by a solver.

	Solvers						
Devices	AQWA	CAPYTAINE	HAMS	NEMOH	NEMOHv3	ORCAWAVE	WAMIT
A_0, A_∞	✓	–	✓	–	–	A_∞	✓
Panel-level info	✓	✓	–	–	–	✓	✓
RAO	✓	✓	✓	–	–	✓	✓
Irreg. frequen.	✓	✓	✓	–	✓	✓	✓
Multi-body	✓	✓	–	–	–	✓	✓
QTF	89	–	–	–	7	897	897
Higher order	–	–	–	–	–	–	✓
License	Comm.	GPL3	Apache2	Apache2	GPL3	Comm.	Comm.
Automation	CLI	Python	CLI	CLI	CLI	–	CLI
GUI	✓	–	–	–	–	✓	–

Table 2
Main dimensions of the devices studied. Note: the Ceto device is fully submerged to a depth of 2.5 m from the top of the device.

	Dimensions			
Devices	Displacement [t]	Length [m]	Beam [m]	Draft [m]
Ceto	2491	25	25	5 (height)
CorPower	282	8.4	8.4	14.4
DeepCWind	14126	67	74	20
ISWEC	458	15	8	4.4
Oyster	227	2.2	18	8.1
ROPAX	16723	184.5	27	6.1
UMaine	20695	90.5	102	20

condition on the body (body condition). This feature makes it easy to use with flexible structures. One of its unique characteristics is that the wave component of the Green function is calculated using interpolation in a look-up table. During its development, it received improvements from F. Rongere, C. McNatt and others. After some years of growth during which time, due to its status as the first, open source, BEM option, NEMOH made a significant impact on the community, its development ceased in 2017 following the retirement of G. Delhommeau and A. Clément. The Laboratoire de recherche en Hydrodynamique, Énergétique et Environnement Atmosphérique (LHEEA) Mercurial repository versions v113 (corresponding to the latest released binaries) and v115 (the latest buildable, which includes improvements in the treatment of irregular frequencies) where the last releases at that time.

Based on the NEMOH codebase, projects OpenWARP and CAPYTAINE were developed: The OpenWARP project begins as a code competition supported by National Renewable Energy Laboratory and the U.S. Department of Energy's Water Power Program, for code that will take a mesh as an input and solves the potential flow problem. After integrating NEMOH, the OpenWARP project improved it by adding it a higher order panel method, so the velocity potential on each panel was not assumed to be constant and equal to the value at the centroid of the panel, but described by a product of two B-splines (Maniar, 1995; Liu, 2009). In addition, simple meshing capability and a graphical user interface were added. The updates to OpenWARP ceased on 2016.

The CAPYTAINE project, although based in old NEMOH Fortran code up to v113, does a deep refactoring of some of the core routines (Ancellin and Dias, 2018), allowing an increased performance due to the use of Intel Math Kernel Library (MKL) and code parallelization using OpenMP. The CAPYTAINE project, initially developed by M. Ancellin and F. Dias at the University College Dublin (UCD) (Ancellin and Dias, 2019), is maintained by M. Ancellin. Since April 2022, it is funded by the Alliance for Sustainable Energy, LLC, National Renewable Energy Laboratory's (NREL) management and operating contractor. CAPYTAINE is limited to first order calculations and cannot handle oscillating water columns or thin members in general. However CAPYTAINE supports multi-body calculations.

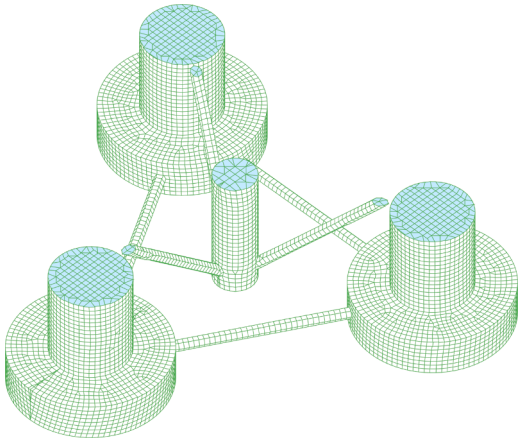

Fig. 2. Example of a mesh where symmetry has been applied and the lid has been obtained. The obtained lid is marked in solid colour, and the cut in the mesh cells due to the symmetry is observable in the xz plane in lower left column.

After a period of time, an ECN team, including R. Kurnia and G. Ducrozet, took up the development of NEMOH, supported by the Horizon 2020 FLOATECH project. As a result, in December 2022, the NEMOH v3.0 was released, with the GPL v3 license, including some improvements: the first-order module allows for removing irregular frequencies using an user-provided lid panel at free surface inside the water piercing bodies, Green's function uses finer interpolation points, new solvers are available for the linear system (LU decomposition and GMRES iterative solver), and a new module is provided for the computation of quadratic transfer functions (QTF) (Kurnia et al., 2022). When using the QTF module, while, for difference-frequency QTF, it is in general acceptable not to compute the free-surface integral terms, for the sum-frequency QTF the user must provide an additional surface mesh which occupies a sufficiently large area around the body water piercing contour (Kurnia and Ducrozet, 2022).

2.4. HAMS

HAMS (Hydrodynamic Analysis of Marine Structures) is an open-source software for the numerical computation of the wave effect on marine structures. It is based on boundary integral equations in the potential flow theory for analysis of wave-structure interactions using a combined source and dipole distribution. It is written in Fortran 90, implementing its computations in parallel using OpenMP. The code has been under development by Yingyi Liu (劉盈溢) at Kyushu University (Japan) for almost a decade. The theory of the panel method as implemented by HAMS is presented in Liu et al. (2016, 2020). The deep-water Green function is included using the Fortran subroutine Green-function-

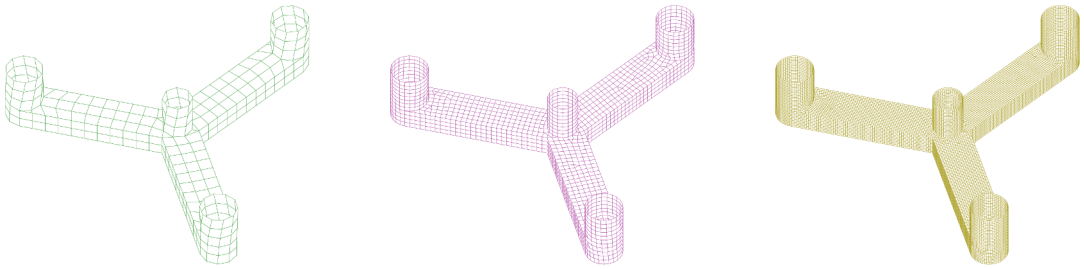

Fig. 3. Examples of the range of discretisations analysed for the same geometry.

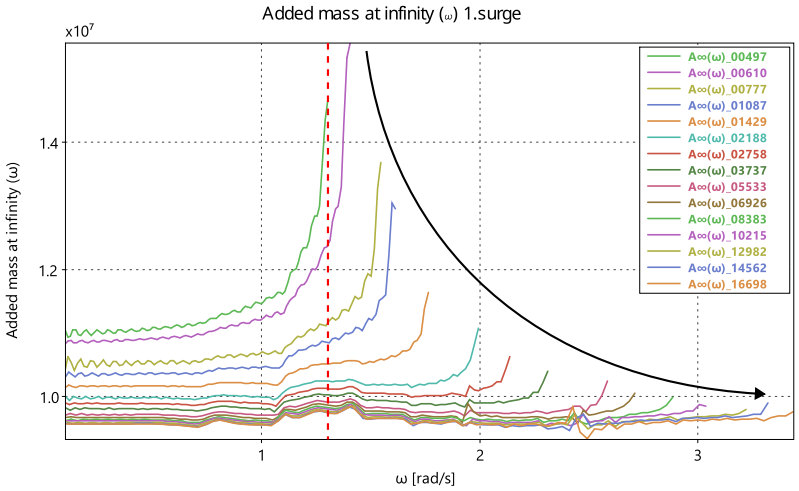

Fig. 4. The results of determining $A_\infty(\omega)$ for each frequency analysed, for the range of discretisations analysed, for the same geometry calculated with AQWA. The red line indicates the minimum frequency range defined by the coarsest mesh The arrow shows the evolution of the results with increasing discretisation.

in-deep-water[1] developed by H. Liang (Wu et al., 2017; Liang et al., 2018). Subsequently, upon the recommendation of Y. Liu, the author made the code publicly available on GitHub to facilitate broader dissemination and accessibility. The finite-depth Green function is using a Fortran subroutine FinGreen3D[2] developed by Y. Liu (Liu et al., 2015).

HAMS includes an option to remove irregular frequencies by enforcing null potential and induced horizontal velocity components at discrete control points on the interior waterplane (Liang et al., 2020; Ohmatsu, 1983). This feature requires an additional water plane mesh to be provided by the user as input when running the simulation.

Some limitations of this software include: it can only handle one body, it does not handle oscillating water columns, and it does not obtain second order forces.

HAMS is freely distributed under the Apache License, version 2.0.

2.5. ORCAWAVE

Developed by Orcina Ltd. in Delphi (a dialect of the Object Pascal programming language) ORCAWAVE was first introduced with the release of OrcaFlex version 11.0 in 2020. ORCAWAVE is included as part of the OrcaFlex license, meaning that OrcaFlex users have access to ORCAWAVE without additional licensing.

2.6. Other software used in this study. BEMRosetta

The realisation of this study, including the automated handling of multiple cases, has required the use of additional software. A brief description is given below.

[1] https://github.com/Hui-Liang/Green-function-in-deep-water
[2] https://github.com/YingyiLiu/FinGreen3D

Table 3
Degrees of freedom considered in the calculation for each of the parameters and devices. Here, 1 to 6, sequentially, represent surge, sway, heave, roll, pitch and yaw.

	Parameters / Degrees of Freedom		
Devices	Added Mass Radiation Damping	Resonance Period	Excitation Force RAO
CorPower	1, 3, 5	3, 5	1, 3, 5
DeepCWind	1, 2, 3, 4, 5	3, 4, 5	1, 3, 5
Ceto	1, 3, 5	–	1, 3, 5
ISWEC	1, 2, 3, 4, 5	3, 4, 5	1, 3, 5
Oyster	1, 5	5	1, 5
UMaine	1, 2, 3, 4, 5	3, 4, 5	1, 3, 5
ROPAX	1, 2, 3, 4, 5	3, 4, 5	1, 3, 5

BEMRosetta (Zabala et al., 2021, 2024) is a software tool which may be used to load, process, visualise, interchange and save different BEM solvers mesh formats, calculations setup files, and hydrodynamic coefficients results. It is developed in C++, and in addition to its sources, it is distributed in a GUI version to be easily handled by users, as a command line tool, as a C++ library, and as a Dynamic-Link library (DLL) to be used from any other software.

This library has been used in this project to create the tool for automatically preprocessing, transforming, and post-processing the cases calculated for the seven different solvers and seven different geometries analysed in this study. Thanks to the use of the BEMRosetta library, the original AQWA meshes are converted into all other mesh formats. Where appropriate, the meshes have been cut for symmetry. New meshes have been obtained by closing the free surface to form a lid for the irregular frequencies removal for solves incorporating this feature, and the AQWA cases are converted into the different calculation setups for each solver. With regard to the output from the solvers, all the results obtained from

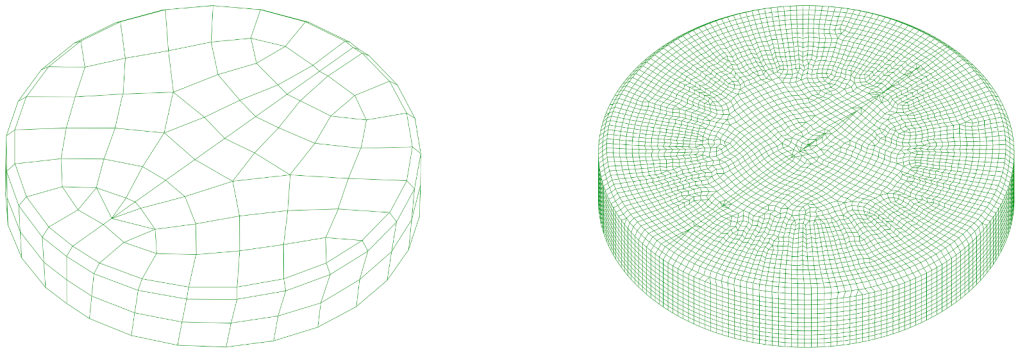

Fig. 5. Coarsest and finest Ceto meshes studied.

the different solvers have been converted into the .out WAMIT format. Without the availability of a library that would allow the realisation and automation of the exchange of mesh files, case definition and hydrodynamic coefficient database, the realisation of the hundreds of cases included in this study would not have been possible, which would have resulted in a study much more limited in scope that the current work.

3. Description of the devices

The following is a brief description of the geometries of the devices and vessel included in this study. The designs included are based on publicly available information, which, in some cases, is not very detailed. Therefore, although the models created meet the requirements of this study, the use of these models to estimate the loads and performance of the real devices and vessel may give different results to those obtained with the highly optimised, original designs created by the respective developers. A sketch of each of the geometries is shown in Fig. 1, and their main dimensions are given in Table 2. A range of geometries with different marine applications were included in the study, comprising proposed floating wind platforms, proposed wave energy converters and a standard sea-going vessel.

3.1. Ceto

The Ceto device, named after a Greek sea goddess, is a submerged point absorber-like wave energy converter, developed by the Australian company Carnegie Clean Energy Ltd. The submerged buoy is anchored to the seafloor and its buoyancy, activated by the passage of waves above it, is used to drive a power take-off. In the current work, the analysed device is a recreation of version 6 of the Ceto device.

3.2. CorPower

CorPower is a surface piercing point absorber-like WEC, with a heaving buoy which is connected to the seabed through a mooring system. The relative movement of the float with respect to the mooring is internally converted into electrical energy by an electromechanical system. It is developed by the Swedish company CorPower Ocean AB. The analysed device herein is a recreation of version C3 of the Corpower device.

3.3. DeepCWind

The DeepCWind semi submersible floating wind substructure was developed for the IEA Wind TCP Task 30 OC4 project (Offshore Code Comparison Collaboration Continued) Phase II (Robertson et al., 2014). It supports the NREL offshore 5-MW baseline wind turbine.

3.4. ISWEC

The ISWEC (Inertial Sea Wave Energy Converter), conceived by the Polytechnic of Turin and developed by Wave for Energy Srl, is a floating WEC which is anchored to the seabed and free to oscillate in pitch in response to the waves. This pitching motion is coupled to the motion of a flywheel and generates a gyroscopic force which is turn acts on generators, which transform the movement into electrical energy. The analysed device is a recreation of the 2019 version of the ISWEC.

3.5. Oyster

Oyster is a wave energy converter conceived by a team led by Trevor Whittaker at Queen's University Belfast and developed by Aquamarine Power Ltd. It consists of a flap attached to the seabed in a very shallow area, such that the top of the device is surface piercing. The flap is hinged near the sea bed and is orientated perpendicular to the swell, so that the flap will oscillate in the direction of wave travel. The model of this device included in this study is based on version 2 of the Oyster. In that version, flap was connected to an energy extraction device, and the energy was transmitted to the shore station for harnessing.

3.6. ROPAX

The acronym ROPAX (Roll-on/Roll-off Passenger) describes a vessel built to carry wheeled cargo that is driven on and off the ship, along with passenger accommodation. Technically this encompasses all ferries with both a roll-on/roll-off car deck and passenger-carrying capacities. The vessel included in this study is a standard conceptual design developed for this occasion.

3.7. UMaine

The University of Maine's (UMaine) VolturnUS-S floating semi-submersible offshore wind turbine reference platform (Allen et al., 2020), is designed to support the IEA 15-240-RWT 15 MW reference wind turbine. This platform is a steel version of UMaine's patented floating concrete foundation technology developed in collaboration with the US Department of Energy.

4. Conditions under which this study was conducted

4.1. General conditions

A particular effort has been made to ensure that the simulations using each of the solvers were carried out under conditions as similar to each other as possible. This was intended to create a level playing field for all the solvers considered, and it was ensured that the following parameters were constant in each case:

- device mesh;
- density, gravity and water depth;
- set of frequencies and headings.

Due to compatibility issues in AQWA with meshes generated by other software, all lower order geometries were modelled using Ansys SpaceClaim, and the mesh coordinates for use with the remaining solvers were obtained from AQWA, through the .dat output file format. Higher order geometries (for use with the WAMIT high-order solver) were modelled using Aerohydro's CAD package, MultiSurf.

Because the Ansys Workbench does not support symmetry, the original meshes include each body in its entirety. However, other solvers included in this study do support certain levels of symmetry, either around the xz plane, the yz plane, or, in some cases, both. This feature allows the calculation time to be greatly reduced. For this reason, and to allow those solvers take advantage of this feature, in the pre-processing phase, meshes of half or a quarter of each body have been generated based on the original meshes. Given that the original meshes are not symmetrical in themselves, cutting the mesh in half to symmetrise it can cause some central cells to become overly slender in shape. This hypothetical handicap has not been significant in practice, as in general the solvers that have used symmetric meshes thus generated have obtained better results than those using the original mesh. To ensure the quality of this operation, the immersed volume of the original mesh has been compared with that of the symmetrised mesh, and it has been found that the volume difference between the original and symmetrised meshes was always below 0.001 %.

Furthermore, some of the solvers included in this study have the capacity to eliminate irregular frequencies through the use of a mesh that closes the inner part of the bodies at the free surface level. While in some solvers this mesh is automatically generated, in others the user is required to provide the free surface mesh externally. In the latter cases, this mesh has been obtained in the pre-processing phase using BEMRosetta. To check the quality of the mesh, the surface area of each of the BEMRosetta-generated surface meshes has been compared with the value of the resulting surface projected on the $z = 0$ plane for the whole body, the error in all cases being less than 0.4 %.

By way of example, Fig. 2 illustrates a mesh used to represent DeepCWind where both the symmetry and the lid has been obtained using BEMRosetta.

The present study includes a comparison of the computational time taken, and Random-Access Memory (RAM) used, by the different solvers in the calculation of multiple discretisations of the same geometry (see Section 7). However, as it was not possible to install all the solvers on the same individual computer, a criterion of scaling the calculation speed between two computers has been developed to allow for direct comparisons to be made between the different solvers. To this aim, due to the fact that it is open source software and hence does not require installation, NEMOH has been taken as the reference software for the computational time and RAM usage comparison. Several simulations have been carried out using NEMOH on all the computers used. By comparing the time taken for corresponding simulations on the different computers a linear adjustment coefficient of calculation speed has been obtained, and this coefficient has been used to scale the speed of calculations of one computer to the speed of the other. With regard to memory, there has been no need to scale, as both computers have RAM memory equal to or greater than 24 Gb, which is sufficient RAM to carry out all simulations included in this study.

4.2. The study benchmark based on higher order mesh

Geometries in BEM solvers can be analysed using either the lower- or higher-order method. When using the lower-order method, the wetted geometry of a body is approximated by an ensemble of flat, quadrilateral panels which are defined by the Cartesian coordinates of each vertex of each panel, and the velocity potential is approximated by piecewise constant values on each panel. In contrast, when the higher-order method is used, panels are not restricted to flat quadrilaterals but may be surfaces with continuous curvature to represent any portion of the body. As such, higher-order panels will result in a more accurate representation of a curved body than lower-order panels. The velocity potential on the body is represented by B-splines in a continuous manner. Using the higher-order method, geometric representations of a body may be generated using a number of approaches, including geometry models created in the surface modelling CAD package developed by Aerohydro Inc, known as MultiSurf (Aerohydro Inc, 2011). The use of the high-order method provides a number of advantages over the lower-order method, notably, the higher-order method converges faster than the low-order method and typically provides a more accurate solution, with a smaller number of unknowns. In this study, higher-order geometries were created using Multisurf. Using the proprietary relational geometry kernel jointly developed by AeroHydro Inc. and WAMIT Inc., WAMIT may directly access and analyse such model geometries. The primary advantage of using this approach is that geometry analysed in WAMIT are fundamentally exact and not compromised by approximations resulting from faceted and NURBS-based geometric representations. For these reasons, the higher-order method in WAMIT is considered the most accurate of all those studied, and hence provides the benchmark against which all other solvers, including the lower-order method in WAMIT, are compared. To further improve the results, the calculations performed with WAMIT high order have a much higher number of panels than the cases with flat panels for each device studied. Of the solvers included in this study, WAMIT is the only one to include an option to use higher-order panels. Details of both the lower- and higher-order approach in WAMIT can be found in Wamit (2023).

4.3. Extent of the calculations performed

Calculations have been carried out for the following discretisations, defined by the number of panels in a model, for each geometry analysed. In addition, seven further cases, one per geometry (with the panel number marked in parenthesis), have been run using the higher order method in WAMIT with a very high number of panels to be considered as benchmarks:

- Ceto: 243, 474, 613, 763, 1062, 1623, 2067, 2389, 2828, 3183, 3627, 4148, 4774, 5552, 5833, 6734, 7454, 8016, 9111, 10,122 (63400).
- CorPower: 274, 320, 419, 555, 716, 974, 1481, 2618, 3081, 3724, 4751 (146800).
- DeepCWind: 2465, 3009, 4064, 7431, 8953, 9964, 11316, 12710, 14474, 17269, 19626, 23,622 (73100).
- ISWEC: 456, 606, 821, 964, 1149, 1400, 1767, 2088, 2372, 2762, 3175, 3855, 4456, 5781, 6988, 8650, 9545, 10914, 12415, 14174, 16,507 (54000).
- Oyster: 429, 440, 594, 626, 742, 870, 1090, 1200, 1435, 1483, 1654, 1925, 2048, 2276, 2896, 3650, 4503, 5891, 7038, 7222, 7699, 8530, 8812, 9772, 10313, 11509, 12,226 (78200).
- ROPAX: 758, 852, 1040, 1208, 1480, 1824, 2224, 2892, 3578, 4192, 4519, 4947, 5427, 6024, 6651, 7422, 8388, 9546, 10917, 12553, 14755, 17387, 20,963 (73550).
- UMaine: 497, 610, 777, 1087, 1429, 2188, 2758, 3737, 5533, 6926, 8383, 10215, 12982, 14562, 16,698 (43225).

The panel numbers used for the different levels of discretisation arise as a consequence of the size of the panels initially used to generate the meshes in Ansys. By performing calculations using each of these discretisations with all 7 solvers in the study, the number of calculations carried out totalled 910. Some of the cases with less satisfactory results have been specially reviewed and repeated to eliminate sources of error which did not arise due to issues with the specific solver itself. Fig. 3 presents some examples of the different mesh discretisation for the same geometry, the Umaine platform.

5. Cause of errors and parameters to detect them

This section deals with the complex issue of selecting the best parameters for a comparative study of this type, and the specific metrics or ratios to be used to demonstrate the quality of each solver. The metrics ultimately used to perform the comparison are described in Section 6. To this aim, the different causes of error that can lead to a solver failing to obtain the best results are first discussed. Subsequently, two possible classes of parameters can be defined, firstly depending on the quality of the internal calculation and secondly depending on the quality of the results. For the class of parameters chosen, the calculation process for each of its parameters and metrics will be detailed afterwards.

5.1. Sources of errors

The goal of the hydrodynamic solvers is to estimate how a specific floating structure design will behave in waves as accurately as possible. Experience has demonstrated that there can be sizeable variations in the hydrodynamic results obtained from different potential flow solvers. Consequently, the subsequent predicted motions can likewise exhibit similar variations between predictions made from the different solvers.

A number of reasons exist to explain these differences (Ittc, 2002):

- Numerical aspects.
- Software engineering aspects, including pre- and post-processing and software quality.

Regarding the first of these points, it must be borne in mind that a numerical model of a general three-dimensional device has to be solved by means of its discretisation. In this discretisation, there are numerous factors to be taken into account:

- Modelling and discretisation of boundary conditions.
- Panel design for surface representation: number of panels, characteristic size and order (flat or curved).
- Calculation methods, especially in the presence of corners and high frequencies.
- Quality and order of the methods used for panel integration.
- Size and accuracy of floating point operations.

A convergence study provides the simplest method for assessing mesh discretisation errors. This is done by comparing the results of a key parameter over successive levels of discretisation to a reference solution (approximating an infinitely refined mesh). The relative error between each discretisation and the reference is calculated, and an acceptable error threshold is set, to determine when the discretisation sufficiently captures the geometric representation. A significant source of numerical error in 3D potential flow simulations is the numerical integration of the Rankine component when evaluating the Green's function over a surface panel. Another example is the error that may arise in calculating tangential velocity at an element using a constant variation of the velocity potential assumption over each panel. This assumption conflicts with finding the tangential velocity at the element, which is the derivative of the velocity potential. The use of Green's second identity to approximate the body surface by plane quadrilateral elements contributes to the error in calculating tangential velocity (Newman and Sclavounos, 1988).

Discretisation errors are influenced by multiple factors such as frequency, wave direction, and object shape. Such errors may have a greater affect on some hydrodynamic coefficients, and at some frequencies, when compared to others. If the panel size is not small enough to capture local variations, errors may occur near edges, corners, and the free surface when analysing drift forces. The panel size should also be small compared to the wavelength to prevent errors. However, in certain situations, the results obtained when increasing the discretisation level may, in fact, converge to incorrect values.

An issue which can arise in the results from BEM solvers is that of so-called "irregular frequencies", which cause erroneous results at certain frequencies. This problem arises from the fact that the panel-based solvers produce a solution for the potential in the vessel hulls' interior and exterior. Numerical solutions will be incorrect close to the Dirichlet eigen-frequencies of the interior domain bounded by the inner surface of the hull and the calm water plane within the hull, even though only the exterior potential is of concern. The estimated coefficients around these frequencies may therefore experience spurious oscillations. The effects of irregular frequencies can be suppressed by placing a "lid" of panels in the calm water plane inside the hull and applying a special boundary condition there (Lee et al., 1996) or, if possible, simply plotting the added mass and damping coefficients as a function of wave frequency and discarding the solutions at the higher frequencies where the peaks are observed. A solution has been proposed to implement this procedure in a more rigorous and automated way (Kelly et al., 2022).

5.2. Study of quality parameters and metrics

In order to perform a comparison between solvers, where not only the quality of the results is considered, but also the speed at which they are obtained, it is necessary to define quality criteria and metrics or ratios to carry out a discretisation analysis. This analysis may take into account in the fact that a solver with more sophisticated calculation procedures can achieve results of equivalent quality to another solver, but with a coarser discretisation. This would allow the more sophisticated solver to obtain results more quickly than a less sophisticated solver, using a finer degree of discretisation, might. Since a user will not normally have several software packages with which to compare results, the value of these ratios has to be defined *a priori*, and has to be as general as possible so such ratios may be fairly applied to different solvers and for the different geometries studied. Two approaches can be used when determining suitable parameters: quality of calculations and quality of results.

5.2.1. Hydrodynamic properties compliance

With Respect to the parameters used for comparing the quality of the calculations, for the different degrees of freedom, and without considering the consequences of the results errors at this time, the following quality criteria may be considered:

- Verification that the added mass and radiation matrices are symmetric and positive semi-definite.
- Presence of unphysical values, such as negative radiation damping.
- Occurrence of spurious oscillations in the hydrodynamic coefficients due to "irregular frequencies".
- Check agreement with Haskind's relation (Newman, 1977; Haskind, 1957; Newman, 1962), which correlates the radiation damping with the integral in all directions of the linear excitation force.
- The application of Haskind's relation in the standard expression of the first order excitation force results in a different but equivalent equation as described in Newman (1977).
- As described in Cummins (1962), Ogilvie (1964), the added mass A_∞ is "genuine" in the sense that it depends only on the body, and it does not depend on the frequency. However, it is observed in practice that the radiation damping and the added mass as a function of frequency, obtained by integration of the surface, do not always agree and may produce non-constant values of A_∞.

Of the above criteria, the first three are not used as metrics in this work due to the difficulty in obtaining a valid key parameter to use with them. With respect to the three remaining parameters, while the mathematical expressions of each are physically identical, in practice, errors of integration can result in differences which can be used to assess the quality of the calculation.

When considering the agreement between the radiation damping from Haskind's relation and that from the radiation potentials, the correct application of Haskind's relation for a non-axisymmetric device requires that the excitation force be calculated for multiple headings such that integration around these gives a sufficiently meaningful result.

For the subsequent criterion, calculation of the excitation forces using the expression derived according to Haskind is required. However, this option is not available for all solvers studied.

Finally, the last criterion above requires only the availability of the added mass and frequency-dependent radiation, which are available in all cases. This increases the value of this parameter. The radiation damping $B(\omega)$ is related to the frequency-dependent component of the added mass $A(\omega)$ through the Kramers-Kronig relations (Kotik and Mangulis, 1962). When concept of impulse response function (IRF), associated with a memory effect caused by the presence of the free surface, is considered, Ogilvie (1964) demonstrated that the IRF can be obtained either using $A(\omega)$ or $B(\omega)$ through the following relations:

$$k(t) = \frac{2}{\pi}\int_0^\infty B(\omega)\cos(\omega t)\mathrm{d}\omega, \tag{1}$$

or

$$k(t) = -\frac{2}{\pi}\int_0^\infty \omega\left(A(\omega) - A_\infty\right)\sin(\omega t)\mathrm{d}\omega. \tag{2}$$

By using a sufficiently well-defined ranged of the radiation damping, $B(\omega)$, the IRF can be obtained from Eq. (1). By combining this with Eq. (2), the following expression for A_∞ can be obtained:

$$A_\infty(\omega) = A(\omega) + \frac{1}{\omega}\int_0^\infty K(t)\sin(\omega t)\mathrm{d}t. \tag{3}$$

Applying Eq. (3) to obtain values for $A_\infty(\omega)$ to each of the meshes with different levels of discretisation, for each frequency analysed, for the UMaine semi-submersible platform calculated with AQWA, results in Fig. 4. It can be observed that for low frequencies, $A_\infty(\omega)$ has an almost constant value. However this value deteriorates with increasing frequency, with the deterioration occurring at lower frequencies the lower the number of panels with which the surface has been discretised. The developers of AQWA are aware of this, and the software will not permit calculations above a frequency that is determined to be of no less than 7 elements over the shortest wavelength. Therefore, in order to obtain a comparison parameter, the smallest frequency range taken from the coarsest discretisation should be taken for all discretisations (marked with the dash red line), so that for all discretisations, for all solvers, the same range is processed. This has been the criterion used in this study, taking for all cases 100 equidistant frequencies within the defined range.

5.2.2. Quality of results

A different approach to defining the parameters and metrics for such a study is to focus on the needs of the users, analysing and measuring the parameters that may be of interest. Although this approach may have less scientific significance compared to the approach described above, given its practical value to users, and also due to the practical impossibility of knowing how the calculations are solved in commercial software due to the lack of source code, it is the one that has been chosen for this study. Given the importance and scope of this topic, it will be dealt with separately in Section 6.

6. Parameters, metrics and results

This section presents a description of the parameters used in the comparison made between solvers in this study. For each parameter, a rationale for its use is provided according to its importance in evaluating the performance of marine devices. In addition, the metrics used to compare parameters, and their detailed calculation procedure, will be defined. The included tables and plots present the results of the study, including the value of the metric and the number of panels of the geometry with which it has been achieved. To save space, this number is given in abbreviated form, with the suffix 'k' indicating thousands of panels. This number is relevant, as two solvers may have obtained similar results, but one may have obtained it with a lower number of panels, which would indicate that this solver for this device converges faster. Since computational issues can result in variations in results for several parameters, in order to avoid repetition, the possible reasons for the deviations uncovered will be left for the end of this section, where in the parameters that are affected will be made clear. It should be noted that metrics are not calculated for all of the geometries analysed for all degrees of freedom, but only for those degrees that are significant and not redundant, due to the nature of the geometries. For example, the results for the yaw mode are not considered for a geometry with xz symmetry. The degrees of freedom analysed for each geometry are included in Table 3. The following is an description of the metrics used, and how they have been applied to the defined parameters.

- The Relative Absolute Error (RAE):

$$\mathrm{RAE} = \left|1 - \frac{y}{y_{\mathrm{ref}}}\right|, \tag{4}$$

  This has been used to compare single values of a parameter. In this equation, y indicates the parameter to be compared and y_{ref} indicates the parameter taken for reference. y_{ref} in some instances may be the result obtained with the best possible discretisation for a solver and a device, while in other instances it may be the result of the calculation taken as a reference.
- Root Mean Square Error (RMSE): In order to compare frequency-dependent parameters, the Root Mean Square Error defined as

$$\mathrm{RMSE} = \sqrt{\frac{1}{n}\sum_{\omega=1}^{n}\left(y(\omega) - y_{\mathrm{ref}}(\omega)\right)^2}, \tag{5}$$

  has been used. As the hydrodynamic coefficients have been calculated for the same frequencies for all solvers and discretisations applied to each geometry, the comparison of values is direct and there was no need to interpolate values. In this study the number of frequencies analysed for a geometry and discretisation, n, is always 100.
- Normalised Root Mean Square Error (NRMSE): As the error results obtained by different parameters are to be compared, they have to be normalised in some manner to ensure a fair comparison. For those parameters that are not, by default, normalised already, such as the RAO, the RMSE has been normalized by dividing it by the average of the reference parameter, as described by

$$\mathrm{NRMSE} = \frac{\mathrm{RMSE}}{\bar{y}_{\mathrm{ref}}}, \tag{6}$$

- Cross Correlation (XCORR): The cross-correlation $\hat{R}_{yy_{\mathrm{ref}}}$ quantifies the similarity between the two curves as a function of their relative displacement. In this study, we compute the normalized cross-correlation (XCORR) as

$$\mathrm{XCORR} = \frac{\hat{R}_{yy_{\mathrm{ref}}}}{\sqrt{\hat{R}_{yy}(0)\hat{R}_{y_{\mathrm{ref}}y_{\mathrm{ref}}}(0)}}, \tag{7}$$

  where normalization ensures that the autocorrelation at zero lag equals unity. This ratio serves as an error metric when comparing a parameter against its reference.
- Root Mean Square (RMS): To aggregate the error rates across all N degrees of freedom, the root mean square error was used and defined as

$$\mathrm{RMS} = \sqrt{\frac{1}{N}\sum_{i=1}^{N} e_i^2}. \tag{8}$$

In order to highlight the results shown, cells with values between 5 and 10 % are displayed in dark yellow and italics, and those with values above 10 % are displayed in dark red and bold.

6.1. Added mass and structural response

6.1.1. Significance of this parameter

In naval devices, the resonance periods of structures are directly proportional to the sum of the mass and the added mass. The accurate analysis of the structural response of a floating platform, for example, must

Table 4
Results of the comparison of the added mass to those obtained with WAMIT using the higher-order method. The number of panels required is also included.

	Solvers						
Devices	AQWA	CAPYTAINE	HAMS	NEMOH	NEMOHv3	ORCAWAVE	WAMIT
CorPower	2.6 % 3k	2.6 % 3k	1.1 % 0k	2.4 % 3k	*6.0 % 3k*	0.7 % 0k	1.0 % 0k
DeepCWind	2.3 % 7k	2.1 % 7k	1.0 % 7k	1.7 % 7k	2.1 % 9k	0.7 % 7k	0.9 % 7k
Ceto	2.4 % 5k	1.9 % 6k	1.3 % 2k	2.3 % 5k	2.3 % 5k	1.0 % 2k	1.2 % 2k
ISWEC	1.6 % 2k	1.5 % 2k	2.3 % 12k	1.3 % 2k	2.0 % 2k	1.3 % 2k	1.3 % 3k
Oyster	**26.2 % 7k**	**15.9 % 12k**	**13.6 % 10k**	**16.8 % 12k**	**44.1 % 9k**	1.9 % 7k	2.5 % 7k
UMaine	1.8 % 6k	1.5 % 6k	1.7 % 6k	1.4 % 6k	1.7 % 6k	1.6 % 6k	1.7 % 6k
ROPAX	2.4 % 17k	2.4 % 4k	1.9 % 4k	2.6 % 4k	**15.2 % 15k**	1.9 % 1k	1.7 % 1k

Table 5
Results of the comparison of the added mass at infinite frequency, compared to that obtained with WAMIT using the higher-order method. The number of panels required is also included.

	Solvers						
Devices	AQWA	CAPYTAINE	HAMS	NEMOH	NEMOHv3	ORCAWAVE	WAMIT
CorPower	2.1 % 3k	2.2 % 3k	0.3 % 0k	2.1 % 3k	2.0 % 3k	0.1 % 0k	0.3 % 0k
DeepCWind	1.4 % 7k	1.6 % 7k	0.5 % 7k	1.6 % 4k	1.7 % 7k	0.5 % 4k	0.5 % 7k
Ceto	1.1 % 5k	1.1 % 5k	0.3 % 2k	1.0 % 5k	1.1 % 5k	0.2 % 1k	0.3 % 2k
ISWEC	0.6 % 2k	0.7 % 3k	1.6 % 12k	0.5 % 1k	0.9 % 2k	0.5 % 2k	0.6 % 3k
Oyster	4.2 % 7k	*6.8 % 2k*	1.9 % 3k	*6.9 % 1k*	*6.5 % 6k*	0.4 % 3k	1.0 % 5k
UMaine	0.7 % 6k	0.8 % 6k	0.8 % 6k	0.6 % 6k	0.7 % 6k	0.9 % 6k	0.9 % 6k
ROPAX	1.3 % 6k	1.4 % 4k	1.8 % 4k	1.7 % 4k	**11.0 % 13k**	1.2 % 1k	1.1 % 2k

be carefully managed to avoid resonance under different excitation frequencies which may arise from incident waves, other environmental forces, or internal frequencies such as those due to the rotational speed of the turbine in the case of floating wind turbines or the rotational speed of the propeller shaft in ships. Resonance effects could render a design unfeasible due to the stresses caused by peak and cyclic loads, which can lead to damage and structural fatigue. Conversely, resonance effects can be desirous for wave energy convertors. For these reasons, the correct determination of the added mass, and hence resonant frequencies is essential for a valid structural analysis and wave energy converter design.

6.1.2. Definition of the metrics

In order to assess the quality of the added mass calculation performed by the solvers, the following three metrics have been investigated:

- $A(\omega)$: **Added mass as a function of angular frequency**
  The RMS of the NRMSE for all degrees of freedom of the added mass has been obtained for the range of frequencies, for each of the discretisations for each solver, comparing with the finest discretisation available for each solver. The chosen mesh is the coarsest mesh that achieves a normalized error of less than 1 %. Once this result has been obtained, the same metric is obtained for the chosen discretisation, but compared with the reference higher order WAMIT model. The results are presented in Table 4.
- A_∞: **Added mass at infinite frequency**
  The RMS of the RAE for the added mass at infinite frequency for each degree of freedom has been obtained, for all the discretisations for each solver. This result is then compared to that for the finest discretisation available for each solver. The added mass at infinite frequency has been obtained using the Eq. (3) for the whole frequency range, averaging the results. The chosen mesh is the coarsest mesh that achieves a normalized error of less than 1 %. Once this mesh has been established, the same metric for this discretisation is compared with the reference higher order WAMIT model. The results are presented in Table 5.
- T: **Resonance period**
  The RMS of the RAE of the resonance period has been obtained for all the degrees of freedom for each of the discretisations for each solver, comparing with the finest discretisation available for each solver.

  The period T is obtained from

$$\omega^2 = \mathbf{C}(\mathbf{M} + \mathbf{A}(\omega))^{-1}, \tag{9}$$

  where $\mathbf{C}$ is the stiffness matrix and $\mathbf{M}$ is the inertia matrix. Each of the degrees of freedom is solved separately, and the diagonal of ω represents the used angular frequency values, converted into periods with $T = 2\pi/\omega$.

  The chosen mesh is the coarsest mesh that achieves a normalized error of less than 1 %. Once this mesh has been established, the same metric for this discretisation is compared with the reference higher order WAMIT model. The results are in Table 6. The period in Ceto is not calculated as it is completely submerged and hence $\mathbf{C} = 0$.

6.2. Radiation damping

6.2.1. Significance of this parameter

The radiation damping quantifies energy dissipation through radiated waves which influences motion responses, especially near resonance. It directly impacts RAO and device stability.

6.2.2. Definition of the metrics

To measure its accuracy, the RMS of the NRMSE of all the degrees of freedom for the radiation damping was obtained for each of the discretisations for each solver, comparing with the finest discretisation available for each solver. The chosen mesh is the coarsest mesh that achieves a normalized error of less than 1 %. Once this mesh has been established, the same metric for this discretisation is compared with the reference higher order WAMIT model. The results are presented in Table 7.

6.3. Excitation forces

6.3.1. Significance of this parameter

The loads received by an offshore device, whether fixed or floating, are largely dependent on the incident wave. These loads can be caused by the excitation effect of the wave due to Froude-Krylov forces, or by

Table 6
Results of the comparison of the resonance period, compared to that obtained with WAMIT using the higher-order method. The number of panels required is also included.

	Solvers						
Devices	AQWA	CAPYTAINE	HAMS	NEMOH	NEMOHv3	ORCAWAVE	WAMIT
CorPower	0.2 % 0k	1.4 % 0k	0.1 % 0k	0.2 % 0k	**12.4 % 3k**	0.1 % 0k	0.1 % 0k
DeepCWind	0.1 % 3k	1.3 % 3k	0.4 % 4k	0.2 % 3k	**21.3 % 17k**	0.4 % 4k	0.4 % 4k
Ceto	–	–	–	–	–	–	–
ISWEC	0.1 % 0k	0.8 % 0k	0.1 % 0k	0.1 % 0k	0.1 % 0k	0.1 % 0k	0.1 % 0k
Oyster	2.0 % 3k	0.6 % 7k	1.2 % 2k	0.4 % 7k	4.7 % 5k	0.0 % 2k	0.1 % 2k
UMaine	0.1 % 3k	1.3 % 3k	0.3 % 4k	0.1 % 3k	1.3 % 15k	0.3 % 4k	0.3 % 4k
ROPAX	0.7 % 1k	1.8 % 1k	0.8 % 1k	**19.9 % 3k**	3.9 % 13k	0.6 % 1k	0.7 % 1k

Table 7
Results of the comparison of the radiation damping to that obtained with WAMIT using the higher-order method. The number of panels required is also included.

	Solvers						
Devices	AQWA	CAPYTAINE	HAMS	NEMOH	NEMOHv3	ORCAWAVE	WAMIT
CorPower	2.1 % 3k	1.6 % 1k	0.9 % 1k	1.4 % 3k	**27.1 % 5k**	0.9 % 1k	1.2 % 1k
DeepCWind	**13.6 % 13k**	*5.0 % 9k*	3.2 % 14k	*9.4 % 9k*	*5.8 % 24k*	2.6 % 10k	2.8 % 11k
Ceto	2.8 % 7k	2.5 % 7k	1.3 % 3k	2.7 % 7k	2.4 % 7k	1.2 % 2k	1.2 % 2k
ISWEC	*5.3 % 9k*	1.2 % 4k	4.1 % 14k	*5.3 % 6k*	1.8 % 4k	0.7 % 4k	0.8 % 4k
Oyster	**27.4 % 7k**	**14.9 % 12k**	**22.3 % 10k**	**15.7 % 12k**	**48.1 % 10k**	2.5 % 7k	2.8 % 9k
UMaine	*5.5 % 8k*	2.0 % 7k	2.1 % 10k	2.4 % 8k	2.3 % 6k	2.1 % 8k	2.1 % 8k
ROPAX	**12.7 % 21k**	2.8 % 4k	1.6 % 7k	4.0 % 10k	**31.9 % 15k**	2.6 % 2k	2.6 % 2k

Table 8
Results of the comparison of the accuracy of the determination of the excitation forces, compared to that obtained with WAMIT using the higher-order method. The number of panels required is also included.

	Solvers						
Devices	AQWA	CAPYTAINE	HAMS	NEMOH	NEMOHv3	ORCAWAVE	WAMIT
CorPower	1.2 % 1k	1.0 % 1k	0.9 % 0k	0.8 % 1k	**20.7 % 5k**	1.0 % 0k	0.8 % 0k
DeepCWind	1.8 % 4k	1.8 % 4k	2.2 % 10k	1.8 % 4k	2.6 % 24k	2.0 % 9k	2.2 % 10k
Ceto	1.8 % 2k	1.5 % 2k	1.1 % 2k	1.6 % 2k	1.4 % 2k	1.2 % 1k	0.9 % 2k
ISWEC	1.6 % 3k	1.0 % 3k	1.7 % 6k	1.7 % 2k	1.5 % 2k	0.7 % 2k	0.8 % 1k
Oyster	**15.6 % 6k**	*9.2 % 12k*	*9.1 % 10k*	**10.1 % 12k**	**25.7 % 7k**	1.6 % 5k	2.0 % 5k
UMaine	1.4 % 6k	1.0 % 6k	1.9 % 7k	1.4 % 4k	1.0 % 6k	1.5 % 8k	1.6 % 8k
ROPAX	2.0 % 1k	1.7 % 10k	2.8 % 4k	2.7 % 6k	**27.8 % 15k**	2.0 % 1k	2.2 % 1k

Table 9
Results of the comparison of the accuracy of the determination of the RAO RMSE, compared to that obtained with WAMIT using the higher-order method. The number of panels required is also included.

	Solvers						
Devices	AQWA	CAPYTAINE	HAMS	NEMOH	NEMOHv3	ORCAWAVE	WAMIT
CorPower	2.2 % 1k	2.8 % 1k	1.0 % 0k	2.1 % 1k	**10.0 % 5k**	2.1 % 0k	0.8 % 0k
DeepCWind	1.4 % 4k	3.2 % 4k	1.3 % 7k	1.6 % 3k	**16.2 % 20k**	2.0 % 7k	1.6 % 7k
Ceto	4.4 % 5k	4.4 % 5k	1.1 % 1k	4.4 % 5k	4.4 % 5k	4.4 % 1k	1.1 % 1k
ISWEC	1.2 % 0k	2.0 % 0k	0.4 % 0k	1.2 % 0k	1.2 % 0k	1.2 % 0k	0.3 % 0k
Oyster	**19.5 % 12k**	4.1 % 12k	**14.6 % 10k**	*6.1 % 12k*	**40.4 % 12k**	2.7 % 12k	2.6 % 7k
UMaine	1.7 % 4k	2.4 % 4k	1.1 % 6k	1.6 % 4k	1.7 % 4k	2.1 % 6k	1.4 % 6k
ROPAX	1.2 % 1k	1.6 % 1k	1.2 % 1k	2.0 % 1k	3.1 % 15k	1.2 % 1k	0.5 % 1k

Table 10
Results of the comparison of the accuracy of the determination of the RAO maximum cross correlation, compared to that obtained with WAMIT using the higher-order method. The number of panels required is also included.

	Solvers						
Devices	AQWA	CAPYTAINE	HAMS	NEMOH	NEMOHv3	ORCAWAVE	WAMIT
CorPower	0.2 % 0k	0.1 % 0k	0.2 % 0k	0.2 % 0k	**12.9 % 5k**	0.6 % 0k	0.4 % 0k
DeepCWind	0.4 % 2k	0.7 % 2k	0.7 % 2k	0.3 % 2k	4.5 % 20k	0.9 % 2k	0.5 % 3k
Ceto	0.1 % 0k	0.1 % 0k	0.0 % 0k	0.0 % 0k	0.2 % 0k	0.0 % 0k	0.0 % 0k
ISWEC	0.1 % 0k	0.0 % 0k	0.0 % 0k	0.0 % 0k	0.0 % 0k	0.0 % 0k	0.0 % 0k
Oyster	0.2 % 1k	1.2 % 1k	1.0 % 1k	0.7 % 1k	0.3 % 1k	0.7 % 1k	0.7 % 1k
UMaine	0.8 % 0k	0.6 % 1k	1.0 % 0k	0.7 % 0k	0.9 % 0k	0.6 % 1k	0.6 % 1k
ROPAX	0.3 % 1k	0.1 % 1k	0.0 % 1k	0.6 % 1k	1.1 % 1k	0.1 % 1k	0.0 % 1k

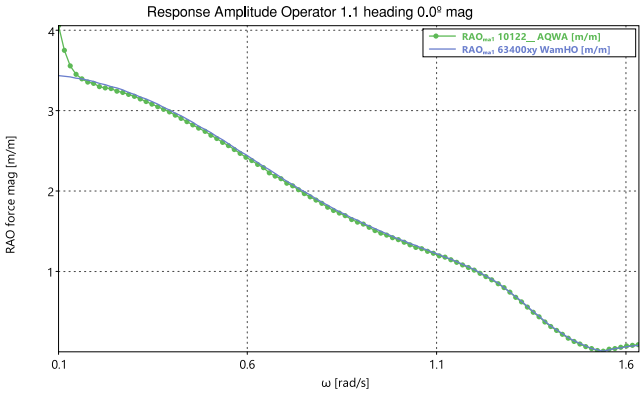

Fig. 6. Ceto surge RAO results showing the divergence in AQWA to the reference solver in low frequencies.

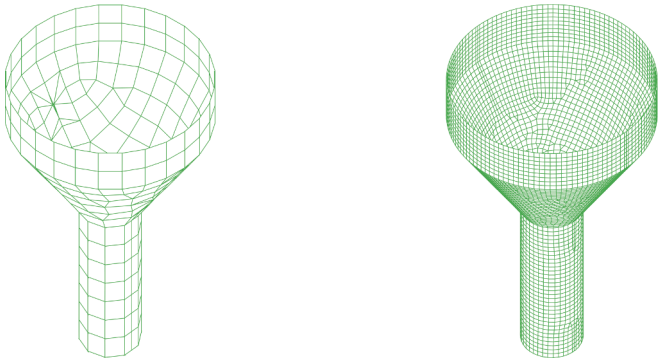

Fig. 7. Coarsest and finest CorPower meshes studied.

the disturbance effect of the device by hindering the passage of the wave, causing diffraction scattering forces.

6.3.2. Definition of the metrics

To measure its accuracy, the RMS of the NRMSE for all the degrees of freedom for the sum of the excitation forces, Froude-Krylov and diffraction scattering was obtained, for each of the discretisations for each solver, compared with the finest discretisation available for each solver. The mesh chosen is the coarsest mesh that achieves a normalized error of less than 1 %. Once this mesh has been established, the same metric for this discretisation is compared with the reference higher order WAMIT model. The results are presented in Table 8.

6.4. RAO

6.4.1. Significance of this parameter

The Response Amplitude Operator (RAO) is the frequency-dependent transfer function that quantifies the amplitude of the response of a floating structure to a unit amplitude wave excitation over a range of frequencies. It has undoubtedly been the most commonly used parameter in comparative studies (see, for example, Silver et al. (2008), Gourlay et al. (2015), Parisella and Gourlay (2016), Mon (2021), Sheng et al. (2022), Raghavan et al. (2022)). This parameter summarizes how the effect of the combination of all phenomena, such as the excitation forces, added masses, radiation dampings, and hydrostatic stiffnesses, affects the response of the device. The RAO is calculated using (Zabala et al., 2021)

$$\mathbf{RAO}(\omega,\theta) = \left[-\omega^2(\mathbf{M}+\mathbf{A}(\omega)) + j\omega\mathbf{B}(\omega) + \mathbf{C}\right]^{-1}\mathbf{F}(\omega,\theta). \tag{10}$$

Note that, in accordance with Eq. (9), the real part of the denominator of Eq. (10), $\mathbf{C} - \omega^2(\mathbf{M}+\mathbf{A}(\omega))$, becomes zero when an object is excited at its resonance frequency. Since, in some cases, the radiation damping at the resonance frequency may be close to zero, the resulting RAO tends to high values at that frequency (Journée et al., 2000). These values, which are several orders of magnitude higher than the rest of the RAO, can distort the results of the applied metrics. As additional damping occurs in real systems (such as viscous damping), a additional damping is often added to the RAO calculation (Malta et al., 2010). In order for this value to be somewhat proportional to the dimensions of the device, the criterion used is that this damping depends on the critical damping considering the system as linear. The standard form of obtaining the critical damping is given by:

$$\mathbf{B}_{\text{crit}}(\omega) = 2\,\mathbf{C}^{1/2}(\mathbf{M}+\mathbf{A}(\omega))^{1/2}. \tag{11}$$

Different experimental tests indicate that a correct damping ratio ζ for various degrees of freedom is between 2 % and 10 % of the critical damping (Simos et al., 2018; Ferrandis et al., 2020). Therefore, a damping ratio $\zeta = 0.05$ (5 %) was applied for this study. With this damping, the modified form of Eq. (10) to obtain the RAO is:

$$\mathbf{RAO}(\omega,\theta) = \left[-\omega^2(\mathbf{M}+\mathbf{A}(\omega)) + \mathbf{C} + j\omega\left(\mathbf{B}(\omega) + \zeta\,\mathbf{B}_{\text{crit}}(\omega)\right)\right]^{-1}\mathbf{F}(\omega,\theta). \tag{12}$$

6.4.2. Definition of the metrics

In order to analyse how well the RAO can be obtained on the basis of the calculated coefficients, the following metrics have been obtained:

- RMSE

  The RMS of the RMSE for all the degrees of freedom for the RAO has been obtained for each of the discretisations for each solver, compared with the finest discretisation available for each solver. The mesh chosen is the coarsest mesh that achieves a normalized error

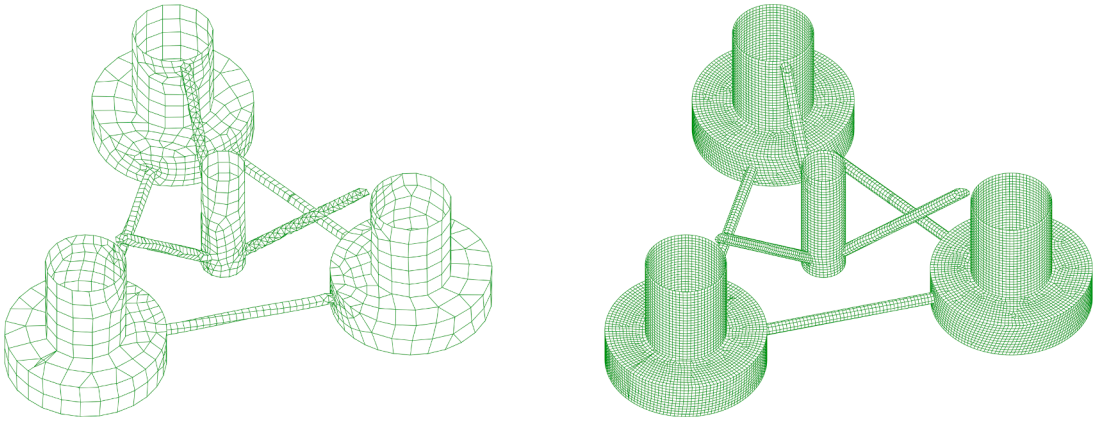

Fig. 8. Coarsest and finest DeepCWind meshes studied.

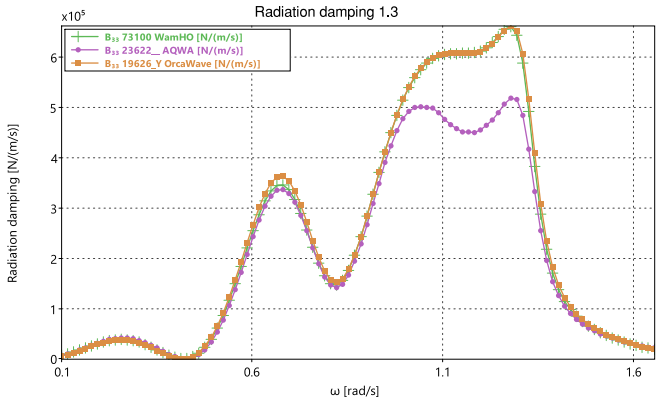

Fig. 9. Heave radiation damping DeepCWind results showing the divergence in AQWA and ORCAWAVE to the reference solver. In this case, the results from AQWA appear to differ from the other solvers across a wide range of frequencies.

of less than 1 %. Once this mesh has been established, the same metric for this discretisation is compared with the reference higher order WAMIT model. The results are presented in Table 9.

- Cross correlation

  The importance of the correlation between the RAO as found using a solver and the reference solver lies in the fact that, when evaluating the RAO, it is not only important to consider the magnitude of the response, but also the frequencies at which the response is greatest. The RMS of the XCORR for all the degrees of freedom for the RAO has been obtained, for each of the discretisations for each solver, comparing with the finest discretisation available for each solver. The mesh chosen is the coarsest mesh that achieves a normalized error of less than 1 %. Once this mesh has been established, the same metric for this discretisation is compared with the reference higher order WAMIT model. The results are presented in Table 10.

6.5. Comments on the results

The solvers have generally given good results as indicated by the chosen metrics, and have proved to be quite insensitive to the very different dimensions and designs studied. This is particularly interesting as some of the metrics used, RMSE and RMS, are quadratic in nature, which would tend to amplify the larger errors in the results. In this section the overall results for each geometry are discussed in turn.

6.5.1. Ceto

The Ceto device comprises a simple geometry, which does not seem to have posed a problem for any solver. Fig. 5 illustrates the difference between the coarsest and finest mesh resolutions. There are some values of the order of 4 % for the RAO as can be seen in Table 9, which is repeated for several of the solvers. Fig. 6. illustrates a comparison of the RAO versus frequency plots obtained for WAMIT using the high order method, and AQWA. A deviation in the results up to a frequency of 0.15 rad/s can be seen, and this, in turn, is due to an variation in the added mass for those frequencies.

6.5.2. CorPower

The visual contrast between the most refined and most coarse meshes is shown in Fig. 7. The errors obtained for this device are in general very small and therefore no further discussion on these results is included herein.

6.5.3. DeepCWind

Fig. 8 presents a side-by-side comparison of the coarsest and finest meshes. The results for this device are also good, although it should be noted that AQWA has a significant deviation in the heave radiation damping at higher frequencies. This deviation is shown in Fig. 9 together with the ORCAWAVE results, which so good agreement with the result obtained from the reference solver.

6.5.4. ISWEC

The disparity in mesh granularity in the versions modelled is depicted in Fig. 10. The results are also good for this device, although in this instance, it should be noted that AQWA has a significant deviation in pitch radiation damping. This deviation is shown in Fig. 11, together with the CAPYTAINE results, which show good agreement with the results obtained from the reference solver.

6.5.5. Oyster

The contours and geometry of the lower order representations of this device are very sensitive to the level of discretisation. The visual contrast between the most refined and most coarse meshes is shown in Fig. 12. In Fig. 13 it can be seen how increasing the discretisation significantly changes the shape of the surface. This sensitivity leads to various errors in several parameters obtained in the solvers, albeit unevenly. For example, Fig. 13 illustrates how increasing the discretisation from 2048 to 12,226 panels in a lower order representation improves the results obtained by AQWA for the radiation damping, but the results from AQWA still show significant divergence from the reference solver. In contrast, the corresponding results obtained by ORCAWAVE, even with a low discretisation, are quite similar to those obtained by the reference solver, and the similarity improves further with increased discretisation.

6.5.6. ROPAX

Despite the complexity of the shapes of this ship, which includes a complex bow to define, the results of all solvers were good for this geometry. Fig. 14 presents a side-by-side comparison of the coarsest and finest meshes. The only issue of note is the appearance of some irregular frequencies in AQWA in the added mass and in the radiation, as can be seen in Figs. 15.

6.5.7. UMaine

Fig. 16 illustrates the difference between the coarsest and finest mesh resolutions. The errors obtained for this device are in general very small and therefore no comments are included herein.

6.6. Summary

The majority of the solvers included in this study have performed satisfactorily. However, in order to facilitate the overall assessment of the results on all the quality parameters analysed, Table 11 includes an average of all the error values for each solver. Aside from the, expected, good result from the low order method in WAMIT, it should be noted that ORCAWAVE has performed almost identically. It should be remembered that since the error admitted by the discretisation in the metrics used is 1 %, the general difference in the results of the two solvers is insignificant compared to those obtained by a higher order solver and with a very high level of discretisation. On the other hand, the open-source solvers HAMS, CAPYTAINE and NEMOH have produced high quality results which compare competitively with the results obtained from the commercial software, for which their authors should be commended. However, the results of NEMOH v3 show that the robustness of that solver has some scope for improvement.

7. Other parameters

Apart from the parameters related to the quality of the results obtained from a given BEM solver, there are other parameters that may be of interest to users, such as computational speed, required RAM resources, and the general robustness of the solver. A number of such parameters are considered in this work. These parameters, and the significance of them, are described below.

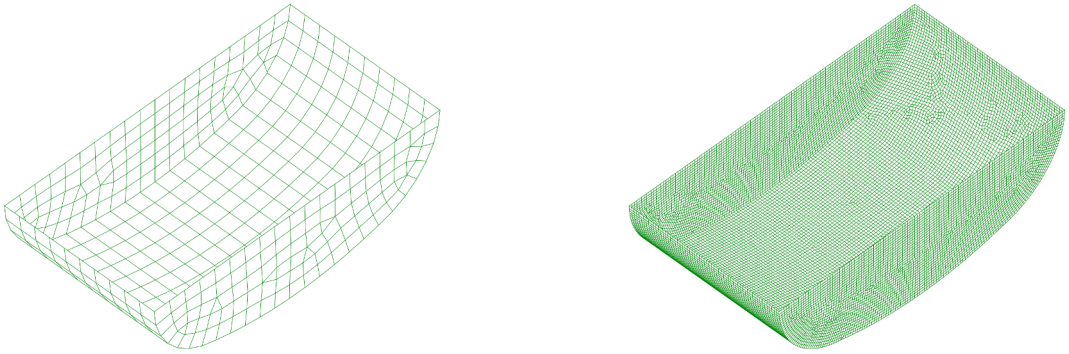

Fig. 10. Coarsest and finest Iswec meshes studied.

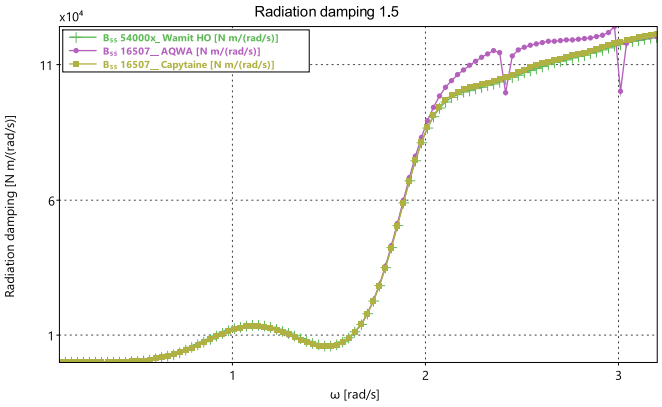

Fig. 11. Pitch radiation damping results comparing the Iswec results of AQWA and CAPYTAINE with the reference solver. In this case, the results from AQWA appear to differ from the other solvers across a wide range of frequencies, including some peaks or irregular frequencies.

7.1. Computation resources

7.1.1. Significance of this parameter

The time required by a solver to complete the analysis of a geometry can be significant. Analyses that take several days to complete may not be feasible in practice, particularly when multiple iterations of a geometry are under investigation. The approach used by a solver to perform the calculations has a major impact on the computation time. Factors such as parallelism in the number of cores used in the computation, proper use of memory, and others, can radically affect the computation time.

The RAM utilisation of a solver can also be an important factor. Memory consumption is usually proportional to the number of panels in the mesh, so a solver with a high memory consumption per panel may be limited in the level of discretisation that can be analysed, leading to poorer quality results.

Potential flow computations are easy to parallelize, since they actually consist of solving as many computations as the number of frequencies to be analysed. So, a solver without in-built parallel computation capabilities can be made to perform parallelised computations simply by dividing the range of frequencies to be analysed into several subranges, effectively distributing the full range of frequencies into several segments, and combining the results at the end. Therefore, in order to make an unbiased comparison between the computational times of the different solvers, the decision was taken to perform the comparison using only one thread per computation (i.e., without the use of parallel processing). Furthermore, so that there is no interference between processes, only one computation was made on a given computer at a time. As this approach is highly time consuming, this comparison was only carried out using one of the geometries, the ROPAX, which was selected due to its geometric complexity.

Since it was not possible to carry out this comparison for all the solvers on a single computer due to the lack of availability of commercial licences, it was carried out on two computers with sufficient resources, adjusting the simulation time used in the comparison on the basis of the average time used on the computers in this study, through several cases analysed using NEMOH v2 with its associated open licence.

7.1.2. Comparison results

Fig. 17 illustrates the results of memory usage and computation time comparison, with the average values presented in Table 12. The values in Table 12 have been obtained by the numerical integration of the results for all solvers up to the number of panels for that solver with the

Table 11
Average results of the combined quality metrics considered in this benchmark.

	Solvers						
Metrics	AQWA	CAPYTAINE	HAMS	NEMOH	NEMOHv3	ORCAWAVE	WAMIT
Average	3.8 %	2.5 %	2.3 %	3.0 %	*9.1 %*	1.2 %	1.1 %

Table 12
Average results of the speed and RAM consumption of a process for each of the solvers, with respect to the results obtained by NEMOH v2. For both parameters, values greater than one indicate whether a solver uses more memory or is slower than NEMOH. Dark yellow cells indicate a specially lower computational speed, and a specially higher memory usage compared to NEMOH v2.

	Solvers						
Speed/RAM	AQWA	CAPYTAINE	HAMS	NEMOH	NEMOHv3	ORCAWAVE	WAMIT
Speed/NEMOH	0.2	*1.7*	0.3	1	0.8	*2*	0.3
RAM/NEMOH	3.1	*15.6*	*14.4*	1	3.1	*21*	2.5

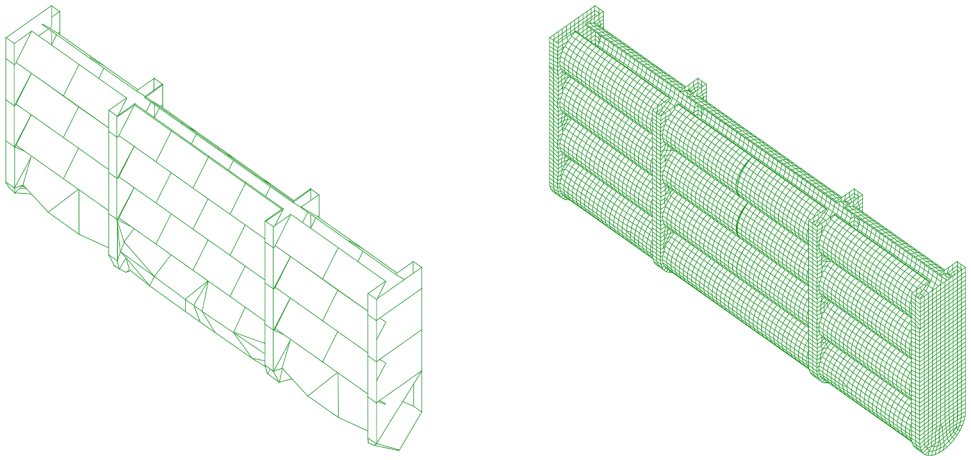

Fig. 12. Coarsest and finest Oyster meshes studied.

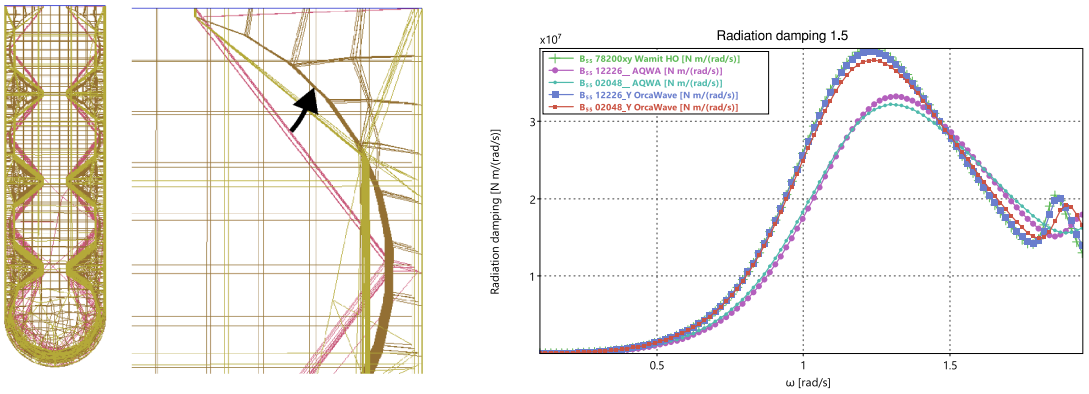

Fig. 13. Effect of the Oyster discretisation highlighted with an arrow showing increasing discretisation (left), and pitch radiation damping results (right) showing the divergence in quality and convergence for some of the solvers. While ORCAWAVE appears to converge rapidly to the results of the reference solver, the results of AQWA do not appear to converge adequately.

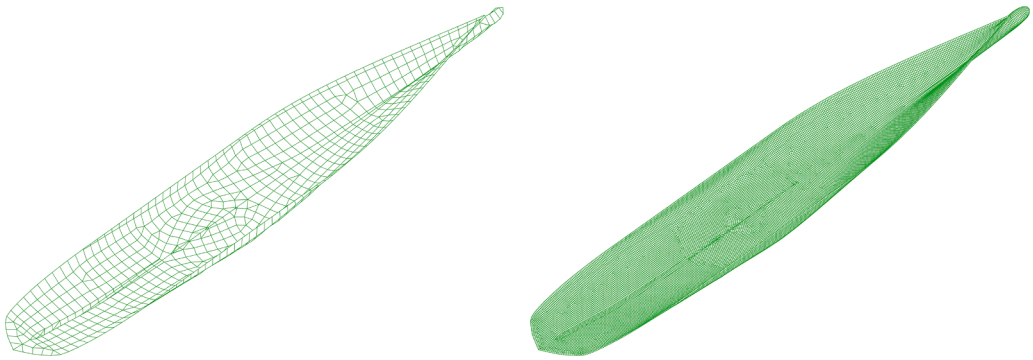

Fig. 14. Coarsest and finest Ropax meshes studied.

Table 13
Results of the comparison of the solver capacity measured using the maximum number of panels that can be solved. In addition, the number of failed calculations is shown as the second value in each cell.

	Solvers													
Devices	AQWA		CAPYTAINE		HAMS		NEMOH		NEMOHv3		ORCAWAVE		WAMIT	
CorPower	4751	0	4751	0	4751	0	4751	0	4751	0	4751	0	4751	0
DeepCWind	23622	0	19626	0	23622	0	14474	0	23622	0	19626	0	23622	0
Ceto	10122	0	10122	0	10122	0	10122	0	10122	5	10122	0	9111	0
ISWEC	16507	0	16507	0	16507	0	8650	0	12415	0	16507	0	16507	0
Oyster	12226	0	10313	0	12226	1	12226	0	12226	0	12226	0	12226	0
UMaine	16698	0	16698	0	16698	1	14562	0	16698	1	14562	0	16698	0
ROPAX	20963	0	17387	0	12553	0	12553	0	14755	4	12553	0	20963	0

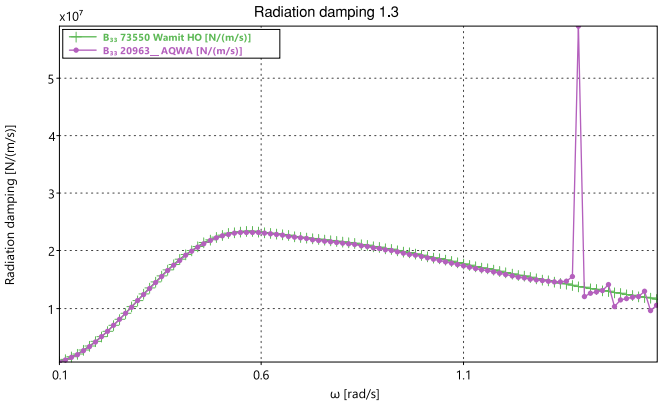

Fig. 15. Heave radiation damping Ropax results showing the divergence in AQWA to the reference solver. In this case, the results from AQWA in high frequencies include some peaks or irregular frequencies.

lowest number of panels. The maximum discretisation of each solver is limited, notably except in the case of AQWA, by the ability to perform its computations without the need for the operating system to paginate memory to disk, as this operation greatly degrades the computational speed, causing the computations to take several days, and distorting the trends found. Because of this, the meshes considered range from 758 to 8388 panels, a range performed by all solvers without the need for the operating system to page RAM to disk due to lack of RAM.

A clear trend between resource consumption and number of panels can be observed in the results with the exception of AQWA, where no relationship between memory usage and number of panels is apparent. To ensure the AQWA results were correct, the AQWA calculations were repeated and, as before, no relationship between memory usage and number of panels was obtained. These results appear to contradict the equation to determine memory usage given in the AQWA documentation, i.e. Memory [Mb] $= 300 + 8\left(\frac{N}{1000}\right)^2$, where N is the maximum number of panels in the simulation. During the AQWA calculations, it was observed that AQWA made frequent use of the hard disk, which might suggest AQWA makes use of its own memory-to-disk paging system, proving to be more efficient than that performed automatically by the operating system. This may be due to the age of the software, designed in an era of scarce computational resources, which forced developers to optimise RAM usage. The opposite is true for other, more modern software developed with higher-level systems, where the ease of obtaining massive computing resources, for example in the cloud, may have focused the developers' priorities on increasing and improving the software's features.

The calculations show that the fastest solver is AQWA, followed by HAMS and WAMIT. With respect to memory usage, the least resource intensive solver is NEMOH v2, possibly partly because it is 32-bit software. For 64-bit software, the least resource intensive solver is WAMIT, followed by AQWA and NEMOH v3.

7.2. Solver capacity

7.2.1. Significance of this parameter

A number of calculations within the range initially proposed for the comparison herein, defined by the number of devices, the number of discretisations considered for each of them and the set of solvers used as described in Section 4.3, were not completed due to problems with the solvers themselves. In some instances, the solver itself indicated out-of-memory problems. Note that these instances are not necessarily for calculations performed for the finest discretisations with the highest number of panels in the geometric representations. In other instances a solver has simply produced completely wrong results when compared to those obtained for the finest discretisations, which might suggest an out-of-memory issue, although not explicitly indicated as such by the solver.

There may be a number of reasons why a solver fails to complete a calculation. The causes may be internal, such as limited memory addressing due to being programmed for a 32-bit CPU, or other internal architecture and matrix sizing limitations due to memory efficiency of algorithms or internal memory management. In particular, these may be imposed by the number of panels in the grid, which defines the size of the numerical resolution systems to be solved.

Although it may be relevant in less efficient program architectures, the number of frequencies and headings chosen is not considered limiting, since they can be solved sequentially, so that the memory used to solve one problem can be freed from the computer's RAM and saved to disk before solving the next problem. Causes of failures may also be external, such as the amount of RAM available. A system with 32 GB of memory was used for these tests, which was found to be sufficient for the WAMIT and AQWA solvers and is therefore considered sufficient for this study.

More significant than the percentage of failed calculations was the average of the maximum number of panels that could be solved in the cases where the calculations failed beyond a certain discretisation.

7.2.2. Comparison results

The results of this comparison are presented in Table 13. The main limitation solvers experience when performing calculations seems to be that of the number of panels in the mesh. However, beyond this limitation, NEMOH v3 and HAMS have shown problems for some models.

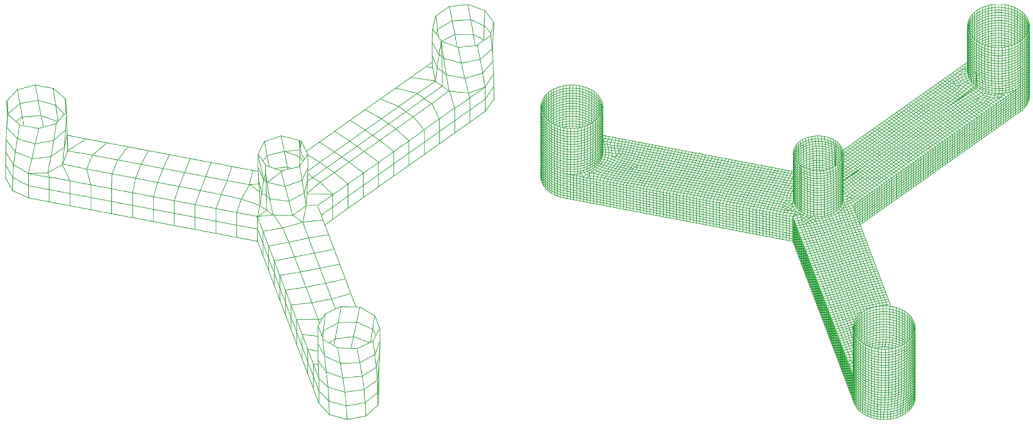

Fig. 16. Coarsest and finest Umaine meshes studied.

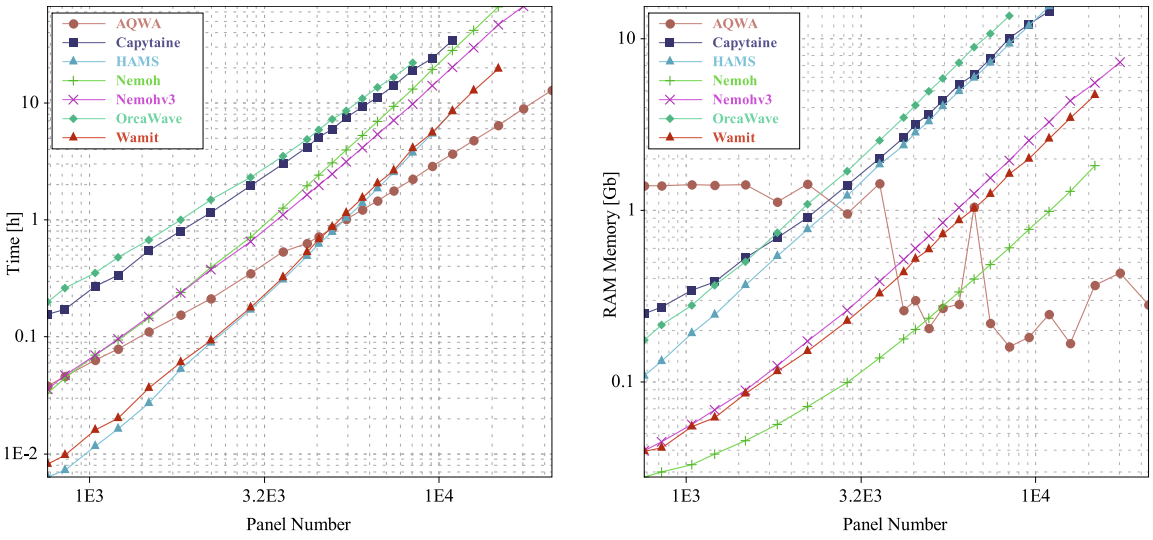

Fig. 17. Simulation time (left) and RAM usage (right) of the study solvers calculating the same case with different discretisation levels. In both cases, exponential growth is observed, linearised by the logarithmic scale of the axes. The only exception is AQWA, which appears to maintain constant memory usage regardless of the mesh size.

AQWA seems to be the most robust solver in this test, although it should be remembered that the meshing tool chosen was from the same vendor.

8. Conclusions

This study presents a systematic and comprehensive benchmark campaign to evaluate the accuracy of linear, frequency-domain Boundary Element Method (BEM) solvers in predicting wave loads and motions of floating and seabed mounted bodies. To quantify these differences, a wide set of 910 test cases involving various marine structures was established and analysed under uniform conditions, covering both simple and complex geometries. The goal is to assess the convergence properties, accuracy and performance of each of the solvers.

Results from multiple BEM implementations were compared against the reference results. For simple geometries, all solvers showed excellent agreement, confirming their ability to capture the correct hydrodynamic behaviour. As the geometrical complexity increased, some variations were observed among the solvers. Nevertheless, these differences were generally within what are deemed by the authors to be acceptable ranges, and convergence was demonstrated as mesh refinement improved the accuracy. In any case, it has been observed that the results obtained by WAMIT and ORCAWAVE have been superior to those of the other solvers, and within the margin of error of the calculations (1 %). Next, and not far behind, HAMS and CAPYTAINE have also shown the best quality results. In terms of calculation speed, AQWA has shown superior speed, followed closely by WAMIT and HAMS. In terms of memory usage, NEMOH v2 has achieved an excellent result, largely based on its 32-bit architecture. Regarding 64-bit solvers, WAMIT obtained a good result, followed by NEMOHv3 and AQWA. The latter maintains memory usage almost independent of mesh size, making it a good option for studying highly discretised meshes.

All input and output files corresponding to the case studies presented in this work, as well as the source code and compiled binaries used for preprocessing and postprocessing, are available in a public repository. The repository can be accessed at Zabala et al. (2025). By offering this open-access information, this study enables reproducibility and facilitates the verification of BEM tools in a transparent manner. It serves both as a snapshot of the current state-of-the-art and as a baseline for future developments. It is therefore expected that this benchmarking will contribute to building user confidence in BEM solvers and support the development of best practices for their application in offshore engineering.

CRediT authorship contribution statement

I. Zabala: Writing – original draft, Software, Investigation, Formal analysis, Conceptualization; **T.E. Kelly:** Writing – review & editing, Investigation, Data curation; **J.C.C. Henriques:** Writing – review & editing, Methodology, Investigation, Formal analysis, Conceptualization; **Y. Peña-Sanchez:** Writing – review & editing, Visualization, Investigation; **M. Penalba:** Writing – review & editing, Resources, Investigation; **J.M. Blanco:** Visualization, Validation, Resources, Formal analysis.

Declaration of competing interest

The authors declare the following financial interests/personal relationships which may be considered as potential competing interests: J.C.C. Henriques reports financial support was provided by Foundation for Science and Technology (FCT, Portugal). Jesus M. Blanco reports administrative support was provided by Basque Government. If there are other authors, they declare that they have no known competing financial interests or personal relationships that could have appeared to influence the work reported in this paper.

Acknowledgments

JCCH acknowledges the Foundation for Science and Technology (FCT, Portugal) for financial support through the LAETA Base Funding project (DOI:10.54499/UIDB/50022/2020). JMB acknowledges the Basque Government for the support given to this research through project IT1514-22. L. García Serradilla (SENER) is acknowledged for the advice, preparation and computation of AQWA and ORCAWAVE calculations.

References

Aerohydro Inc , 2011. Aerohydro Multisurf® User Manual. Southwest Harbor, Maine.

Allen, C., Viscelli, A., Dagher, H., Goupee, A., Gaertner, E., Abbas, N., Hall, M., Barter, G., 2020. Definition of the UMaine VolturnUS-S Reference Platform Developed for the IEA Wind 15-MegaWatt Offshore Reference Wind Turbine. https://www.osti.gov/biblio/1660012.

Ancellin, M., Dias, F., 2018. Using the Floating Body Symmetries to Speed Up the Numerical Computation of Hydrodynamics Coefficients with Nemoh. Vol. 9. American Society of Mechanical Engineers. https://doi.org/10.1115/omae2018-77924

Ancellin, M., Dias, F., 2019. Capytaine: a Python-based linear potential flow solver. J. Open Source Software 4 (36), 1341. https://doi.org/10.21105/joss.01341

Babarit, A., Delhommeau, G., 2015. Theoretical and numerical aspects of the open source BEM solver NEMOH. In: Proceedings of the 11th European Wave and Tidal Energy Conference (EWTEC2015), pp. 1–14. https://hal.archives-ouvertes.fr/hal-01198800.

Bertram, V., Söding, H., Graf, K., 2006. PDSTRIP - A strip method for ship and yacht seakeeping, In: 9th Numerical Towing Tank Symposium Le Croisic.

Buchner, B., Dijk, A., Wilde, J., 2001. Numerical multiple-body simulations of side-by-side mooring to an FPSO. In: Proceedings of the International Offshore and Polar Engineering Conference.

Chen, X., 1993. Evaluation de la fonction de Green du problème de diffraction/radiation en profondeur d'eau finie: Une nouvelle méthode rapide et précise. In: Actes des 4e Journées de l'Hydrodynamique pp. 371–384.

Cummins, W.E., 1962. The impulse Response Function and Ship Motions. Technical Report. Navy Department, David Taylor Model Basin.

Delhommeau, G., 1989. Amelioration Des performances Des codes De calcul De diffraction-radiation au premier ordre. In: Actes de la 2ème Journées de l'Hydrodynamique Nantes, France, pp. 69–88.

Ferrandis, J.A., Bonfiglio, L., Rodríguez, R.Z., Chryssostomidis, C., Faltinsen, O.M., Triantafyllou, M., 2020. Influence of viscosity and non-linearities in predicting motions of a wind energy offshore platform in regular waves. J. Offshore Mech. Arct. Eng. 142 (6), 62003. https://doi.org/10.1115/1.4047128

Gourlay, T., Graefe, A.V., Shigunov, V., Lataire, E., 2015. Comparison of AQWA, GL Rankine, MOSES, OCTOPUS, PDSTRIP and WAMIT with model test results for cargo ship wave-induced motions in shallow water. Prof. Robert F. Beck Honoring Symp. Marine Hydrodyn. Am. Soc. Mech. Eng. 11, 1–10. https://doi.org/10.1115/omae2015-41691

Haskind, M., 1957. The exciting forces and wetting of ships in waves. Izvestia Akademii Nauk S.S.S.R., Otdelenie Tekhnicheskikh Nauk, No. 7, English Translation 1962 by J. N. Newman Available as David Taylor Model Basin 1045 Translation No.307.

ITTC, 2002. Recommended Procedures and Guidelines. Validation of Seakeeping Computer Codes in the Frequency Domain. https://ittc.info/media/1315/75-02-07-024.pdf.

Jonge, P.D., Peters, P., Huismans, H., 2008. A hydrodynamic analysis method for offshore discharge operations. In: Proceedings of OMAE, pp. 188–196.

Journée, J.M.J., Massie, W.W., Hydromechanics, O., Delft, T.U., 2000. Offshore Hydromechanics, TU Delft, https://ocw.tudelft.nl/wp-content/uploads/OffshoreHydromechanics_Journee_Massie.pdf.

Kelly, T., Zabala, I., Peña Sanchez, Y.P., Penalba, M., Ringwood, J.V., Henriques, J.C.C., Blanco, J.M., 2022. A post-processing technique for removing 'irregular frequencies' and other issues in the results from BEM solvers. Int. Mar. Energy J. 5 (1), 123–131. https://doi.org/10.36688/imej.5.123-131

Kotik, J., Mangulis, V., 1962. On the Kramers-Kronig relations for ship motions. Int. Shipbuild. Prog. 9 (97), 361–368. https://doi.org/10.3233/isp-1962-99701

Kring, D., Korsmeyer, T., Singer, J., Danmeier, D., White, J., 1999. Accelerated, nonlinear simulations for large structures. In: Proceedings of the 7th International Conference on Numerical Ship Hydrodynamics, pp. 1–4.

Kurnia, R., Ducrozet, G., 2022. NEMOH v3.0 User Manual. https://www.researchgate.net/publication/366166860_NEMOH_v30_User_Manual.

Kurnia, R., Ducrozet, G., Gilloteaux, J.C., 2022. Second Order Difference- and Sum-Frequency Wave Loads in the Open-Source Potential Flow Solver NEMOH. Vol. 5. American Society of Mechanical Engineers. V05AT06A019. https://doi.org/10.1115/omae2022-79163

Lee, C.H., Newman, J.N., Zhu, X., 1996. An extended boundary integral equation method for the removal of irregular frequency effects. Int. J. Numer. Methods Fluids 23 (7), 637–660. https://doi.org/10.1002/(sici)1097-0363(19961015)23:7<637::aid-fld437>3.0.co;2-3

Liang, H., Wu, H., Noblesse, F., 2018. Validation of a global approximation for wave diffraction-radiation in deep water. Appl. Ocean Res. 74, 80–86. https://doi.org/10.1016/j.apor.2018.02.025

Liang, H., Housseine, C.O., Chen, X., Shao, Y., 2020. Efficient methods free of irregular frequencies in wave and solid/porous structure interactions. J. Fluids Struct. 98, 103130. https://doi.org/10.1016/j.jfluidstructs.2020.103130

Liang, H., Chen, X., 2025. Boundary element method for wave interactions with marine structures: from conventional to emerging applications. Eng. Anal. Bound. Elem. 179, 106326. https://doi.org/10.1016/j.enganabound.2025.106326

Liu, Y., 2009. Fast Multipole Boundary Element Method. Cambridge University Press.

Liu, Y., Iwashita, H., Hu, C., 2015. A calculation method for finite depth free-surface Green function. Int. J. Naval Archit. Ocean Eng. 7 (2), 375–389. https://doi.org/10.1515/ijnaoe-2015-0026

Liu, Y., Hu, C., Sueyoshi, M., Iwashita, H., Kashiwagi, M., 2016. Motion response prediction by hybrid panel-stick models for a semi-submersible with bracings. J. Mar. Sci. Technol. 21 (4), 742–757. https://doi.org/10.1007/s00773-016-0390-1

Liu, Y., Cong, P., Gou, Y., Yoshida, S., Kashiwagi, M., 2020. Enhanced endo's approach for evaluating free-surface Green's function with application to wave-structure interactions. Ocean Eng. 207, 107377. https://doi.org/10.1016/j.oceaneng.2020.107377

Maniar, H.D., 1995. A three-dimensional higher-order panel method based on B-Splines. Technical Report. Massachusetts Institute of Technology. Ph.D. thesis.

Martin, P.A., Rizzo, F.J., 1861. On boundary integral equations for crack problems. Proc. R. Soc. London A. Math. Phys. Sci. 421, 341–355. https://doi.org/10.1098/rspa.1989.0014

Malta, E.B., Gonçalves, R.T., Matsumoto, F.T., Pereira, F.R., Fujarra, A.L.C., Nishimoto, K., 2010 Damping coefficient analyses for floating offshore structures 29th International Conference on Ocean, Offshore and Arctic Engineering: Volume 1. Vol. 29. pp. 83–89. https://doi.org/10.1115/OMAE2010-20093

Mctaggart, K., 2011. Verification and validation of shipmo3D ship motion predictions in the time and frequency domains. Int. J. Naval Archit. Ocean Eng. 3 (03). https://doi.org/10.3744/JNAOE.2011.3.1.086

Mon, E.P.S., 2021. A Comparative Study Between Diffraction Analysis Softwares and Measured Motions. Technical Report. Université de Liège. Belgique. Master's thesis.

Naciri, M., Sergent, E., 2009. Diffraction/Radiation of 135,000 m^3 Storage Capacity LNG Carrier in Shallow Water: A Benchmark Study. Offshore Technology, ASMEDC Vol. 1. pp. 637–647. https://doi.org/10.1115/omae2009-79645

Newman, J.N., 1962. The exciting forces on fixed bodies in waves. J. Ship Res. 6 (04), 10–17. https://doi.org/10.5957/jsr.1962.6.4.10

Newman, J.N., 1985. Algorithms for the free-surface Green function. J. Eng. Math. 19 (1), 57–67. https://doi.org/10.1007/bf00055041

Newman, J.N., 1977. Marine Hydrodynamics. The MIT Press. https://doi.org/10.7551/mitpress/4443.001.0001

Newman, J.N., Sclavounos, P.D., 1988. The computation of wave loads on large offshore structures. In: Proc. 5th. Conf. on the Behaviour of Offshore Structures (BOSS '88), pp. 1–18.

Ogilvie, T.F., 1964. Recent progress toward the understanding and prediction of ship motions. In: Proceedings of the 5th Symposium on Naval Hydrodynamics, pp. 3–80.

Ohmatsu, S., 1983. A New Simple Method to Eliminate the Irregular Frequencies in the Theory Water Wave Radiation Problems. Technical Report. Papers of Ship Research Institute.

Parisella, G., Gourlay, T.P., 2016. Comparison of open-source code Nemoh with Wamit for cargo ship motions in shallow water. Technical Report. Centre for Marine Science and Technology, Curtin University.

Penalba, M., Giorgi, G., Ringwood, J.V., 2017a. Mathematical modelling of wave energy converters: a review of nonlinear approaches. Renew. Sustainable Energy Rev. 78, 1188–1207. https://doi.org/10.1016/j.rser.2016.11.137

Penalba, M., Kelly, T., Ringwood, J., 2017b. Using NEMOH for modelling wave energy converters: a comparative study with WAMIT. In: Proceedings of the 12th European Wave and Tidal Energy Conference (EWTEC2017), pp. 1–10. http://mural.maynoothuniversity.ie/12466/.

Raghavan, V., Lavidas, G., Metrikine, A., Mantadakis, N., Loukogeorgaki, E., 2022. Trends in renewable energies offshore. In: Proceedings of the 5th International Conference on Renewable Energies Offshore (RENEW 2022). CRC Press, pp. 441–447. Ch A comparative study on BEM solvers for Wave Energy Converters. https://doi.org/10.1201/9781003360773-50

Robertson, A., Jonkman, J., Masciola, M., Song, H., Goupee, A., Coulling, A., Luan, C., 2014. Definition of the Semisubmersible Floating System for Phase II of OC. Technical Report. National Renewable Energy Laboratory. https://doi.org/10.2172/1155123

Sheng, W., Tapoglou, E., Ma, X., Taylor, C.J., Dorrell, R.M., Parsons, D.R., Aggidis, G., 2022. Hydrodynamic studies of floating structures: Comparison of wave-structure interaction modelling. Ocean Eng. 249, 110878. https://doi.org/10.1016/j.oceaneng.2022.110878

Silver, A., Hughes, M., Conrad, R., Lee, S., Klamo, J., Park, J., 2008. Evaluation of Multi-Vessel Ship Motion Prediction Codes, Tech. Rep., Naval Surface Warfare Center Carderock Div Bethesda MD Ship Hydromechanics Dept.

Silver, A.L., Hughes, M.J., 2010. A method of evaluating multi-vessel surface effect ship motion prediction codes. In: Proceedings of the 2010 Conference on Grand Challenges in Modeling & Simulation, GCMS '10, Society for Modeling & Simulation International, pp. 239–246.

Simos, A.N., Ruggeri, F., Watai, R.A., Souto-Iglesias, A., Lopez-Pavon, C., 2018. Slow-drift of a floating wind turbine: an assessment of frequency-domain methods based on model tests. Renew. Energy 116, 133–154. https://doi.org/10.1016/j.renene.2017.09.059

Söding, V.B.H., 2009. A 3-d Rankine source seakeeping method. Ship Technol. Res. 56 (2), 50–68. https://doi.org/10.1179/str.2009.56.2.002

Wamit, 2023. Vol. 11. https://www.WAMIT.com/,online.

Weems, K., 2007. LAMP-MULTI: A LAMP Version for Multiple, Interacting Bodies in Waves User's Guide. version 3.1.2 edition edition.

Wu, H., Zhang, C., Zhu, Y., Li, W., Wan, D., Noblesse, F., 2017. A global approximation to the Green function for diffraction radiation of water waves. Eur. J. Mech. B. Fluids 65, 54–64. https://doi.org/10.1016/j.euromechflu.2017.02.008

Zabala, I., Henriques, J.C.C., Kelly, T.E., Ricci, P.P., Blanco, J.M., 2024. Post-processing techniques to improve the results of hydrodynamic boundary element method solvers. Ocean Eng. 295, 116913. https://doi.org/10.1016/j.oceaneng.2024.116913

Zabala, I., Kelly, T., Henriques, J.C.C., Penalba, M., Peña-Sanchez, Y.P., Blanco, J.M., 2025. Dataset and code for "Boundary element methods in action: A performance assessment for engineering applications". https://doi.org/10.5281/zenodo.15737067

Zabala, I., Peña-Sanchez, Y.P., Kelly, T., Henriques, J.C.C., Penalba, M., Faedo, N., Ringwood, J.V., Blanco, J.M., 2021. BEMRosetta: an open-source hydrodynamic coefficients converter and viewer integrated with NEMOH and FOAMM. In: Proceedings of the 14th European Wave and Tidal Energy Conference (EWTEC2021), pp. 2124–2125.